©GRAPHIC STOCK

Habib Zaidi and
Minerva Becker

The Promise of Hybrid PET/MRI

Technical advances and clinical applications

During the last few decades, positron emission tomography (PET)-based molecular imaging has advanced elegantly and steadily gained importance in the clinical and research arenas. However, the lack of structural information provided by this imaging modality motivated its correlation with structural imaging techniques such as X-ray computed tomography (CT) or magnetic resonance imaging (MRI), which are well established in the clinical setting. The additional capability of simultaneous acquisition of PET and MRI data bridges the gap between molecular and morphologic diagnoses. Since diagnostic imaging methods evolve from the anatomical to the molecular level, the mission of multimodal and multiparametric imaging increasingly becomes more essential. Since 2010, whole-body hybrid PET/MRI has been investigated in the clinical setting for clinical diagnosis and staging, treatment response monitoring, and radiation therapy treatment planning of a wide range of malignancies. However, quantitative PET/MRI is still challenged by the lack of accurate and robust attenuation and motion compensation strategies to enable the production of artifact-free and quantitative PET images. This article briefly summarizes the historical development of PET/MRI and gives

Digital Object Identifier 10.1109/MSP.2015.2482225
Date of publication: 27 April 2016

an overview of the state of the art and recent advances in the design and construction of clinical systems. Progress in quantitative imaging, including MRI-guided image reconstruction and correction, and potential clinical applications of this novel technology are also discussed.

Introduction

PET is considered to be one of the key molecular imaging modalities enabling noninvasive characterization and quantitative evaluation of a multiplicity of molecular and physiologic biomarkers in vivo at the cellular level in healthy and disease states, including neurology, psychiatry, cardiology, and oncology. However, PET produces blurred and noisy images that inherently lack the anatomical information required for localization of metabolic abnormalities. This limitation has motivated the combination of PET with structural imaging modalities, such as X-ray CT and MRI. Currently, PET is capitalizing and complementing other anatomical imaging modalities, such as CT and MRI, to address basic research and clinical questions. However, multimodality imaging requires robust registration of images generated by various modalities. Initially, multimodality imaging was accomplished through the use of software-based image registration (rigid body or deformable) and fusion to correlate anatomical and molecular information [1]. However, the challenges and inherent limitations of software-based image registration approaches motivated the emergence of hardware-based approaches for multimodality imaging. The advent of combined PET/CT and PET/MRI systems, their commercial introduction, and the fast and wide acceptance of the former in the clinic have had a significant impact on patient management and clinical research. However, the latter is still an "embryonic" technology, having the potential to become a powerful tool and likely to play a pivotal role in clinical diagnosis and research [2], [3].

This article reviews the state-of-the-art developments and the latest advances in hybrid PET/MRI instrumentation along with quantitative procedures developed to address the challenges of this modality. An outlook outlining potential promising developments and current and future clinical applications of this technology is also discussed.

History of hybrid PET/MRI

The history of PET/MRI can be traced back to 1986, when the first attempts to perform PET imaging within strong static magnetic fields were initiated, motivated by the need to reduce positron range prior to annihilation through magnetic confinement of emitted positrons [4], [5]. Indeed, the static magnetic field of the MRI subsystem influences the trajectory of positrons, causing them to spiral between successive interactions with matter, thus reducing the in-plane spatial resolution of the PET subsystem. Monte Carlo simulation studies demonstrated that the use of a magnetic field collinear with a PET scanner's axis improves the transaxial spatial resolution without impinging on the axial spatial resolution [5]. For instance, Wirrwar et al. [6] reported foreseen improvements in spatial resolution for high-energy positron-emitting tracers ranging between 18.5% (2.73 mm instead of 3.35 mm) for ^{68}Ga and 26.8% (2.68 mm instead of 3.66 mm) for ^{82}Rb at a field strength of 7 T. Another effect, which has been characterized only very recently, is the degradation of the axial spatial resolution owing to the elongation of the positron range distribution along the magnetic field B0 or the so-called shine-through artifact [7]. It was reported that this effect might cause severe artifacts in PET images for malignant lesions located close to air cavities, particularly when using high-energy positron-emitting radionuclides (see the section "Pitfalls and Artifacts").

Contrary to the history of PET/CT, which began with the design of hybrid systems suitable for clinical use, PET/MRI began with systems dedicated to preclinical imaging. Surprisingly, the history of hybrid PET/MRI instrumentation per se can be traced back to 1995, prior to the introduction of PET/CT [8]. Early designs of MR-compatible PET detector modules focused on modifying detector blocks of an existing small-animal PET scanner to avoid mutual interference by placing photomultiplier tubes (PMTs) at a realistic distance from the strong magnetic field of a clinical MRI unit [9]. For the sake of avoiding or reducing mutual interference between imaging modalities, the coupling of detector blocks, position-sensitive PMTs, and readout electronics located outside of the magnetic field was achieved through long (4–5 m) optical fibers. The main disadvantage was, however, the nonnegligible loss of scintillation light through the long fibers, resulting in a weak signal, which negatively impacts energy and timing resolution, impairs deteriorating crystal identification, and decreases PET signal performance, reducing overall PET performance [10].

Although this design concept bears inherent limitations, analogous approaches were adopted in academic settings [11]. Other associated approaches based on conventional PMT-based PET detectors included split-magnet [12] and field-cycled [13] MRI, which rely on more complex magnet designs. In the split-magnet design, an 8-cm gap in the axial direction of a 1-T magnet enables accommodation of the microPET Focus 120 small-animal PET scanner (Siemens Healthcare, Erlangen, Germany) and 1.2-m-long optical fiber bundles [12], making it possible to place the PMTs at very low field strength (~30 mT). The main advantage of this design is the need for only minor modifications of conventional PET detectors and associated readout technologies, although the magnet and gradient coil design is more complex and costly compared with technologies used on current-generation MRI systems. In the field-cycled design, PMTs are assembled into the magnet, although PET data acquisition is barely permitted within short time intervals (~2.5 seconds) when MRI polarizing and readout fields are switched off [13]. The challenges associated with this design still need to be addressed before a viable hardware realization can be achieved. Moreover, the need for electromagnets instead of conventional superconducting magnets requires noteworthy compromises.

The introduction of MR-compatible readout technologies, such as avalanche photodiodes (APDs) and silicon photomultipliers (SiPMs), was essential to achieve this goal.

Avalanche photodiode-based readout technology was successfully employed on a commercial preclinical scanner [14] and various prototypes for small-animal [15] and breast [16] PET/MRI. Small pixelated APDs or SiPMs operated in "Geiger mode" and more recent readout technologies, such as analog [17] and digital [18] SiPMs, have been investigated as possible candidates for PET/MRI, and their current performance is sufficient for the design of combined PET/MRI systems [19], given that the bulk of MRI electronics could be significantly reduced [20]. Convincing experimental results and in vivo mouse images obtained on APD-based PET/MRI design demonstrate the capability for simultaneous PET/MRI [15]. More importantly, experimental measurements confirmed that each subsystem performs equally well when the other is on or off, reinforcing that each modality is barely visible to the other. These technological advances motivated additional exploration of the clinical potential of PET/MRI [21].

Design considerations of hybrid PET/MRI systems

Contrary to sequential PET/CT, where the design concept is straightforward and consists of putting together two separate modalities, the design of fully integrated PET/MRI systems is less obvious. Indeed, such development requires not only modifications of the PET subsystem to deal with MR compatibility but also significant redesign of the MRI subsystem [3], [10], [22]. Basically, two major design concepts for PET/MRI have emerged: sequential and concurrent [23] (Figure 1). In the former design concept, a serial arrangement of two separate scanners enables sequential data acquisition of both modalities using a single patient's bed to transfer the patient from one modality to the other. Conversely, the latter consists of either an MR-compatible PET insert that can be placed with the MRI gantry or a compact integrated system enabling truly simultaneous data acquisition.

The sequential design is the more straightforward and by far the more economical concept, requiring only minor modifications of both subsystems (e.g., shielding the PET detectors) and arranging for a common patient bed. Sequential PET/MRI systems were designed in anticipation of the availability of mature and economically viable simultaneous whole-body PET/MRI systems, which appeared later and became commercially available. Two design concepts have materialized depending on the configuration adopted for patient bed shuttling from one modality to the other. Systems belonging to the first category include the Ingenuity TF PET/MRI system (Philips Healthcare, Best, The Netherlands), in which a common sliding/rotating bed transfers the patient from MRI to PET and vice versa [24]. The PET/CT/MR trimodality imaging system (GE Healthcare, Little Chalfont, United Kingdom) consists of commercial PET/CT and MRI systems placed in separate but nearby rooms, and a specially designed patient transfer tabletop, docked on both imaging systems, is used to shuttle the patient from the PET/CT to MRI examination rooms [25]. A similar design concept dedicated to brain imaging was pursued by Cho et al. [26] by docking a high-resolution research tomograph and 7-T MRI.

The concurrent design of hybrid PET/MRI is possibly more attractive but is technically more challenging because it involves addressing many difficulties to deal with space restrictions and to avoid interference between the two modalities. To this end, MR-compatible photodetector technologies that are insensitive to magnetic fields and readout electronics producing the least amount of heat radiation have to be used [10]. In addition, the PET detector modules should not affect the operation of the MRI subsystem through electronic interference with the radio frequency (RF) and gradient coils. In essence, the operation of both modalities should not be affected by their integration, and both subsystems should retain their full performance, similar to what can be achieved with two separate PET and MRI scanners.

As mentioned in the previous section, recent developments in solid-state detectors have led to the replacement of conventional PMTs by MR-compatible position-sensitive APDs and SiPMs for the practical implementation of fully simultaneous PET/MRI systems. The PET insert concept, consisting of placing the detector ring inside an MRI scanner,

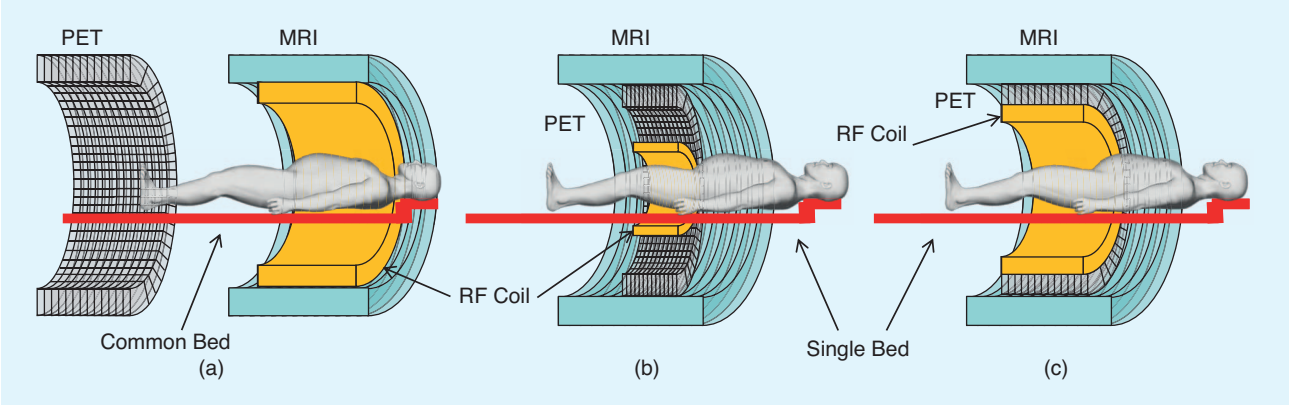

FIGURE 1. Schematic cross-sectional views of potential designs for combined PET/MRI systems: (a) a tandem design with two imagers mounted back to back (similar to that in PET/CT instrumentation) to allow sequential rather than simultaneous acquisition, (b) an insert design with the PET imager inserted between the RF coil and gradient set of the MR imager, and (c) a fully integrated design with two imagers in the same gantry. The RF coil, gradient set, PET imager, and patient bed are shown for all configurations. (Figure adapted with permission from [23].)

was the first landmark, and a number of studies have described different design trends, focusing particularly on the integration of small-bore, small-animal PET scanners inside existing clinical MRI scanners. The small diameters of these devices allows them to fit into the MRI system without crowding the MRI gradients.

As mentioned previously, fully integrated compact systems combining PET and MRI components in a single apparatus, such as Siemens Healthcare's Biograph mMR and GE Healthcare's SIGNA, constitute the most promising design concept for PET/MRI. The exploitation of the most advanced technologies available for both systems is advised to achieve the best performance. For instance, using a PET scanner equipped with time-of-flight (TOF) capability is certainly a bonus, as discussed in the following section. In this regard, SiPMs have many advantages compared with other solid-state photodetectors, such as APDs, because they have better performance characteristics, including high gain, signal-to-noise ratio (SNR), and timing resolution, enabling the implementation of TOF PET on potential PET/MRI systems.

Instrumentation for clinical PET/MRI

The successful design of small-animal PET/MRI systems spurred the development of clinical systems, with the first prototype (called BrainPET) for brain imaging manufactured by Siemens Healthcare in collaboration with the University of Tübingen in Germany [27]. The system performance was characterized and its suitability for various clinical applications assessed at a number of academic institutions. Special attention was paid to the possibilities offered by high-resolution structural MRI, including high soft-tissue contrast sensitivity and advanced functional MRI techniques [28]. A sequential PET/MRI system was also developed to meet the needs of molecular and genetic brain imaging by docking separate PET and 7-T MRI scanners together with a shared common bed for interscanner patient translation [26].

Subsequent to early groundbreaking developments, different design concepts of PET/MRI systems have materialized during the last decade in both academic and corporate settings. Figure 2 shows photographs of current commercial clinical whole-body PET/MRI systems with potential design concepts. Table 1 summarizes the main characteristics of clinical PET/MRI systems developed so far.

The Ingenuity TF PET/MRI system, with TOF Gemini TF PET and Achieva 3T X-series MRI systems, is one such example, allowing for sequential acquisition of aligned PET and MR images. A number of such systems were deployed worldwide, and the PET subsystem was fully characterized using

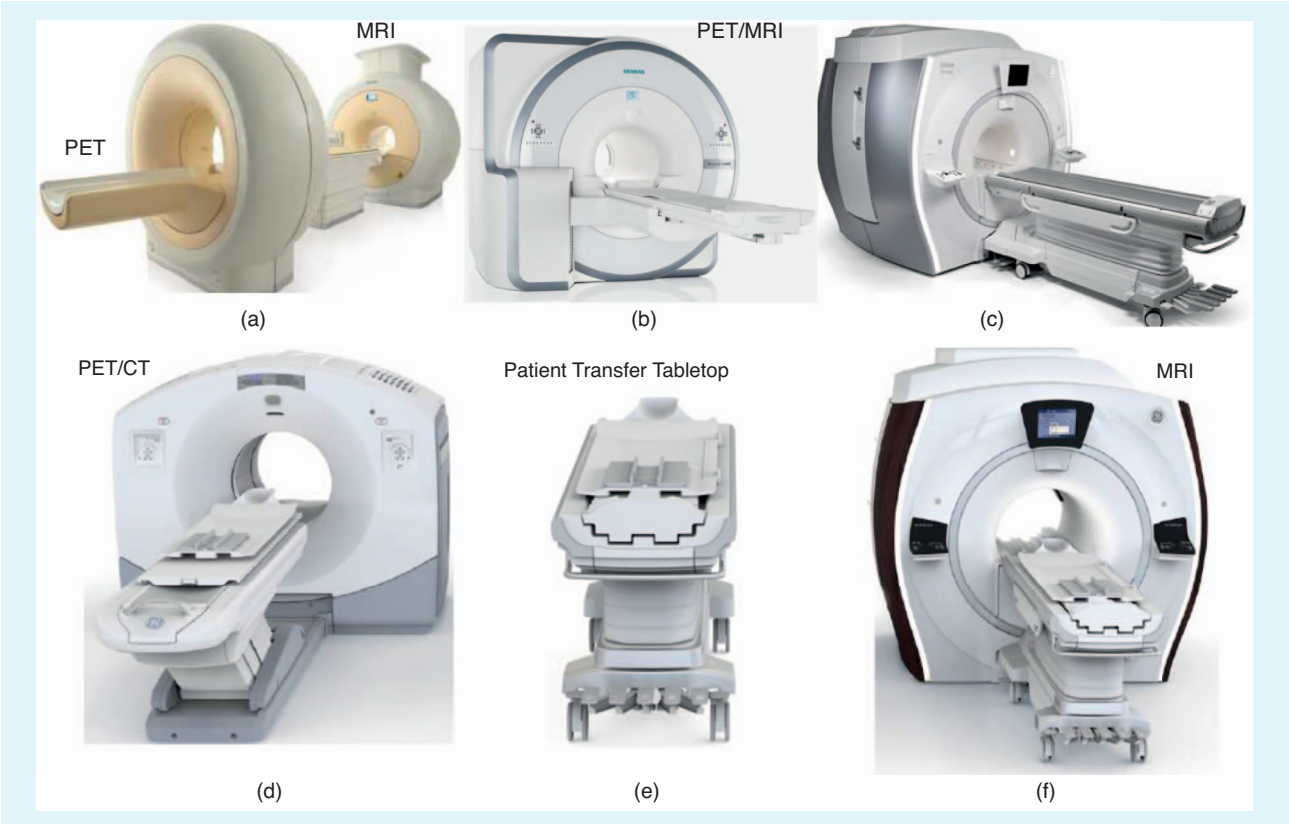

FIGURE 2. (a)–(c) The Philips Healthcare whole-body Ingenuity TF PET/MRI system [in which a turntable patient-handling system facilitates patient motion between the PET subsystem shown in (a) and the Achieva 3T X-series MRI system shown in (c) for sequential acquisition], the Siemens Healthcare Biograph mMR system, and the GE Healthcare SIGNA PET/MRI system, enabling simultaneous acquisition of PET and MRI data. (d)–(f) The GE Healthcare trimodality (PET/CT and MRI) setup using a dedicated patient transporter tabletop. [(a) and (c) used courtesy of Philips Healthcare, (b) courtesy of Siemens Healthcare, and (d)–(f) courtesy of GE Healthcare.]

Table 1. The main features of currently available clinical PET/MRI systems.

System	Manufacturer	Operation	PET detector/readout	Axial FOV (cm)	TOF	MRI	Reference
Biograph mMR	Siemens Healthcare	Simultaneous	LSO/APDs	25.8	No	Verio 3T (modified)	[29]
Ingenuity TF	Philips Healthcare	Sequential	LYSO/PMTs	18	Yes	Achieva 3T	[24]
Signa PET/MRI	GE Healthcare	Simultaneous	LYSO/SiPMs	25	Yes	MR750w 3.0T (modified)	[17]
Trimodality	GE Healthcare	Sequential	LYSO/PMTs	15.7	Yes	MR750w 3.0T	[25]
BrainPET	Siemens Healthcare	Simultaneous	LSO/APDs	19.2	No	Trio 3T (modified)	[30]
Brain MGI	Academia	Sequential	LSO-LYSO/PMTs	25.2	No	Magnetom 7T	[26]

Adapted with permission from [23].

the National Electrical Manufacturers Association (NEMA) NU 2-2007 standard, demonstrating that its performance was not compromised by the presence of the strong MR magnet [24]. Most performance parameters were comparable to those reported for the commercial Gemini TF PET/CT system.

The design concept of the concurrent BrainPET was further exploited to build the Siemens Healthcare Biograph mMR whole-body PET/MRI system, which was also installed in a relatively large number of institutions [29]. More recently, a simultaneous PET/MRI system (SIGNA) based on MR-compatible SiPMs and enabling the implementation of TOF capability was introduced in the market by GE Healthcare [17].

Most current PET/MRI systems have been tested within a high field and proved to produce PET and MR images that appear to be free of distortion, confirming the premise that the interference between the two systems is almost negligible and that each modality is practically invisible to the other [17], [24], [27], [29], [30]. Switching clinical workflows to PET/MRI introduces a number of image registration challenges that were not of major concern with traditional PET/CT scanners. These relate to the additional artifacts within MRI, such as bias fields, the range and number of MRI sequences, and the range of fields of view (FOVs) and orientations of the acquired images [31].

During the last decade, hardware and software advances have enabled improved localization of the position of annihilation along the line of response. The precise measurement of the difference between the arrival times of the two annihilation photons, referred to as TOF, enables more accurate localization of the annihilation point. However, the annihilation point could be located only with limited precision owing to inherent uncertainty in the detector modules and readout electronics, causing some ambiguity in the photon arrival times. As such, the incorporation of TOF information in the image reconstruction process enables improved SNR and tumor detectability in addition to reduction of patient scanning time and/or injected dose, all depending upon patient size and coincidence time resolution (CTR). The SNR improves as the CTR decreases, and this improvement becomes more significant for overweight patients. In a clinical setting, this results in a more homogeneous image quality across different (and increasing) patient sizes and overall yields a much-improved image quality in shorter acquisition times, thus providing the possibility to investigate novel acquisition protocols, such as whole-body dynamic imaging. The SNR gain when using TOF is equivalent to a non-TOF image reconstructed using higher statistics; in this way, adding TOF information to PET increases the sensitivity of the scanner. In addition, TOF PET scanners are less sensitive to inaccuracies in normalization and data correction procedures, including attenuation compensation [32]. The first commercial TOF PET/MRI scanners using lutetium oxyorthosilicate (LSO)/lutetium-yttrium oxyorthosilicate (LYSO) crystals and PMT/SiPM photodetectors have a time resolution of 400–600 picoseconds [17], [24]. APD-based hybrid PET/MRI systems, including the BrainPET and Biograph mMR scanners, are not equipped with TOF capability owing to the poor timing resolution of APDs. A CTR of fewer than 100 picoseconds has been obtained with short crystals of 3–5 mm [33], [34]. The interaction length of 511-keV photons in LSO is 12 mm. As such, achieving a sensible detection efficiency requires 15–20-mm-long crystals. However, the CTR degrades with increasing length owing to the reduction in the speed of light in the high refractive index of the scintillator because the position along the length of the crystal where the interaction of the 511-keV photon occurred is unknown. With advances in detector technology and fast electronics, a TOF PET/MRI scanner with sub-100-picosecond CTR will likely be possible in the near future (Figure 3). The target in the long term is to attain the physical limit of spatial resolution for clinical scanners (~2 mm), and by definition, a target CTR of 20 picoseconds would be required to obviate the need of image reconstruction.

Hybrid small-animal PET/MRI is also flourishing in both academic and corporate settings, with several prototypes based on different design concepts and a number of companies already offering commercial solutions [15], [22]. The potential benefits of compact and integrated systems were already recognized, and it is expected that this technology will find a niche in preclinical research, which is well under way [35].

Quantitative PET/MRI

PET/MRI shows promise for radiotracer uptake quantification via image fusion of molecular and structural data to assist in anatomical localization of functional abnormalities

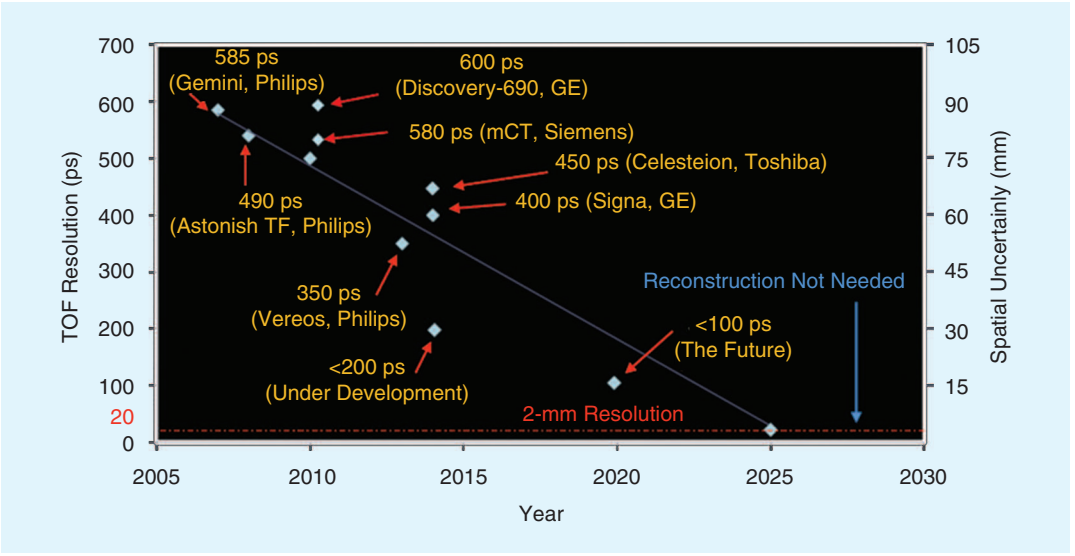

FIGURE 3. The evolution of TOF resolution performance characteristics of current-generation and future-generation TOF PET scanners. PS: picoseconds.

and delineation of regions of interest (ROIs) for quantitative analysis. However, there are several challenges undermining the widespread adoption of this technology, which may, in fact, represent inherent limitations. Similar to CT in PET/CT, MRI provides the structural information suitable for implementation of attenuation compensation techniques and introduction of a priori anatomical information into image reconstruction, partial-volume correction, and motion correction schemes. However, contrary to PET/CT, in which CT-based attenuation correction is straightforward, MRI-guided attenuation correction is challenging and still requires further development [36]. Owing to its clinical relevance and the challenges faced, the latter issue is addressed in more detail in this article.

MRI-guided attenuation correction in PET/MRI

The development of MRI-guided attenuation correction algorithms has received considerable attention during the last decade. This was motivated by the lack of space in PET/MRI systems, precluding placement of external radionuclide sources within the gantry. MRI-guided attenuation correction is, however, still in its infancy and remains extremely challenging for whole-body imaging. The impact of this limitation on clinical interpretation of findings and patient outcome is not yet clear.

MRI-guided attenuation correction is complex because MRI signal intensity is not correlated with electron density, thus making conversion of signal intensity to attenuation coefficients complicated (Figure 4). MRI-guided attenuation map derivation consists of locating and mapping various biological tissues with different attenuation properties in the body. This can be achieved by one of the three main categories of techniques: 1) MRI segmentation-based techniques, in which the body is segmented into regions corresponding to tissues/organs with different attenuation properties, followed by assignment of corresponding linear attenuation coefficients at 511 keV to the segmented tissues/organs; 2) atlas-based and machine-learning

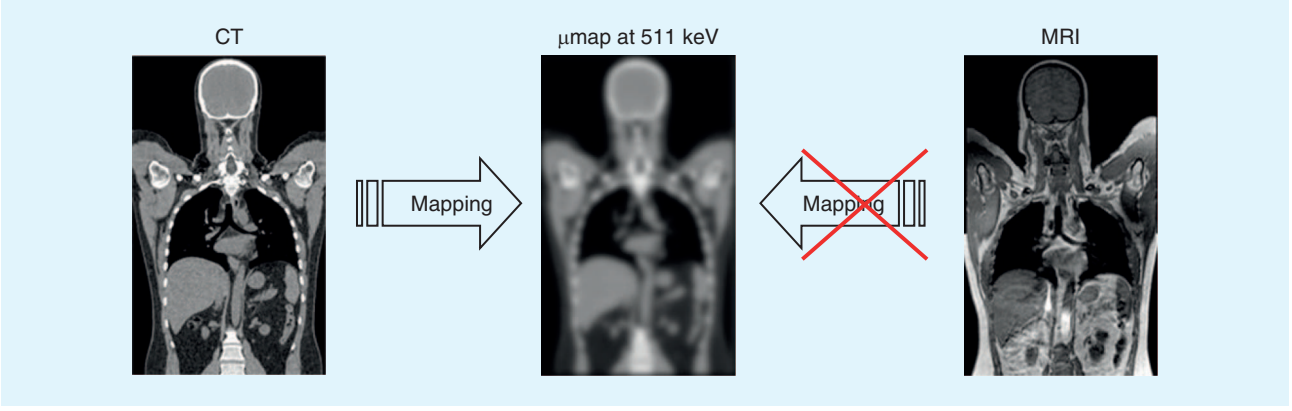

FIGURE 4. The conversion of CT images (Hounsfield units) to an attenuation map at 511 keV is evident (in the absence of sources of error), whereas the MR intensity level is not directly related to electronic density, which renders the conversion of MR images to attenuation maps less evident compared with CT.

techniques, in which an aligned MR/CT atlas combined with a learning strategy enables the prediction of the pseudo-CT from an actual patient's MR image; and 3) emission-based and transmission-based algorithms, in which the TOF emission or transmission data are exploited to derive the attenuation map (Figure 5) [37].

Segmentation-based methods are simple to implement and usually require a single and fast MRI sequence. However, they suffer from limited accuracy in the determination of attenuation coefficients owing to the limited number of segmented clusters (usually three to five, including air, lungs, fat, soft tissue, and fat/nonfat mixture) and the assignment of theoretical rather than actual patient-specific attenuation coefficients. In these techniques, bones and air pockets are replaced by soft tissue, and the variability of attenuation coefficients is ignored, especially in the lungs. Tissues such as bone and lung and various pathological abnormalities with varying attenuations are among the most challenging in whole-body imaging. With the exception of the use of ultrashort echo time [38] and zero echo time [39] pulse sequences, cortical bone has very low signal intensity on conventional MRI sequences and is difficult to distinguish from air cavities and gas in the body. These sequences were designed to portray tissues with low proton density and short T2 relaxation time (e.g., cortical bone and lungs) and, as such, to separate the bone signal from soft tissue. The main drawback of these techniques is the long acquisition time and susceptibility to artifacts when using a large FOV, which limits their application to only brain imaging [37]. A number of studies have shown that ignoring bone might not be adequate for quantification of osseous lesions with bias in estimation in tracer uptake [standardized uptake value (SUV)], varying between 5 and 15% in most cases but going up to 30% in some cases [40]–[45].

The second category of approaches consists of using representative anatomical atlas registration, in which an MRI template is registered to a patient's MRI, and prior knowledge of the atlas attenuation properties, obtained by registration to a corresponding CT template combined with a learning algorithm based on the use of support vector machines, is applied to derive a patient-specific attenuation map [46]. Reliable deformable registration algorithms play a pivotal role in this approach, and failure of the registration process in the case of large deformations will produce incorrect results [47]. The critical issue is the extent to which the global anatomy depicted by an atlas will predict individual and patient-specific attenuation maps. For this and a few other reasons, most techniques proposed so far that belong to this category were developed specifically for brain imaging [48], [49]. Adaptation of these techniques for whole-body imaging applications required few modifications to be made, consisting mainly of generating a four-class segmentation of the MR images to improve the registration process and optimal selection of

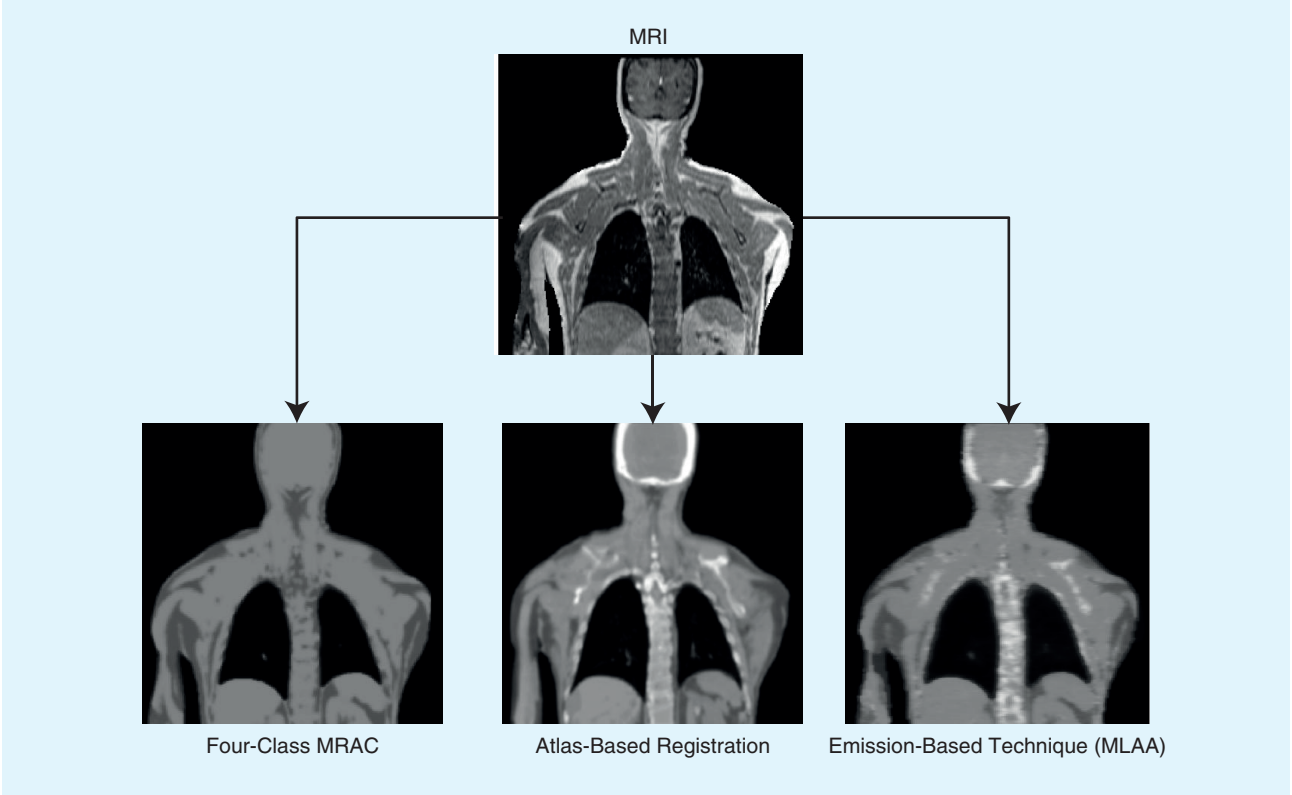

FIGURE 5. Strategies for MRI-guided attenuation map generation, including the four-class segmentation-based method, atlas-based registration and machine learning, and MRI-guided emission-based technique (MLAA). MRAC: MRI-based attenuation correction. (Figure adapted with permission from [37].)

regions for the learning process and applying postprocessing techniques to determine the tissue class for which sufficient information is available from the MRI. In a more recent contribution, Arabi and Zaidi [50] improved the robustness of the aforementioned technique [46] to nonsystematic registration bias and anatomical abnormalities by discarding locally gross misalignment errors from the training and pseudo-CT generation process through local sorting of the atlas images using the local normalized cross-correlation criterion as a metric to assess the similarity to the target image prior to providing it to the training step. Despite promising preliminary results reported in a number of studies using more advanced approaches [48], [50], more research is still required to make the procedure completely automated and suitable for clinical usage in whole-body PET/MRI.

Emission-based techniques form the last category of algorithms and have gained substantial momentum during the last decade. They are now recognized as valuable approaches for estimation of the attenuation map in PET/MRI through the simultaneous estimation of activity and attenuation within a maximum-likelihood (MLAA) framework [51]. However, these techniques suffer from cross-talk, depend on tracer distribution, and are susceptible to counting statistics. The use of TOF information proved to partially mitigate the cross-talk issue and stabilize the joint estimation problem [52]. It is worth emphasizing that TOF PET is less sensitive to attenuation artifacts than conventional non-TOF PET. Recent advances in emission-based techniques demonstrated the promise of an MRI-guided MLAA algorithm for attenuation correction in whole-body PET/MRI [53]. In this work, the estimation of attenuation maps takes advantage of a constrained Gaussian mixture model and Markov random field smoothness prior imposed by MRI spatial and CT statistical constraints. These techniques proved to outperform previous approaches reported in the literature [54]. Overall, each category of techniques has its own pros and cons, and it is expected that hybrid techniques combining at least two (and ideally the three categories of attenuation correction methods) will result in more accurate and robust techniques.

The many other challenging issues that still have to be addressed in this regard, including attenuation of MRI hardware (tables, rigid and non-rigid RF coils, pillows, headphones, medical probes, and other objects that are MRI-invisible but contribute to photon attenuation), patient positioning aids in the FOV, and conductive MR-compatible or nonconductive but MRI-invisible implants, should also be taken into account. Another challenging issue is transaxial plane truncation owing to the limited MRI FOV, which results in incomplete attenuation maps, producing artifacts on corresponding attenuation-corrected PET images.

MRI-guided image reconstruction in PET/MRI

One of the important limitations of statistical iterative reconstruction techniques, such as the maximum-likelihood–expectation-maximization (ML–EM) algorithm, is that a large number of iterations deteriorate image quality and amplify noise in PET images [55]. An elegant way to control the noise characteristics consists of incorporating a prior distribution to depict the statistical properties of the image to be determined and thus generate a posteriori probability distributions from the image conditioned upon the data [10]. The well-established Bayesian reconstruction framework forms a prevailing expansion of the popular ML–EM algorithm. The maximum a posterior (MAP) estimate is derived from maximization of the a posteriori probability over the set of probable images [56]. There are many benefits associated with this approach in the sense that the diverse mechanisms of the prior, including the pseudo-Poisson nature of statistics, nonnegativity of the solution, local voxel correlations, or identified presence of anatomical boundaries (from correlated structural imaging), may be incorporated into the estimation process, evaluated independently, and employed during the algorithm's implementation [10]. Prior anatomical information obtained from correlated anatomical imaging can also be included in PET reconstruction within a Bayesian framework to avoid resolution loss resulting from regularization, albeit to recover resolution by taking advantage of the better resolution of anatomical images [57]. This has been achieved with various degrees of success over the years using MRI [58].

A coupling term is usually incorporated in this category of reconstruction techniques, which favors the preservation of edges in PET images related to the location of relevant anatomical boundaries extracted from corresponding anatomical images. A Gibbs prior distribution is typically used to encourage the piecewise smoothness of PET images, which can be included in the Bayesian model. Promising preliminary results were reported by various investigators using segmentation-free anatomical priors based on similarity measures analogous to mutual information, but further research and development efforts are still required. Therefore, the advent of simultaneous hybrid PET/MRI systems creating perfectly aligned molecular and anatomical images is stimulating the further development and assessment in the clinical setting of Bayesian MAP reconstruction algorithms.

As an example, a MAP algorithm for PET image reconstruction incorporating MRI information with joint entropy between PET and MRI features serving as the regularization constraint was proposed [59]. A nonparametric method was then used to estimate the joint probability density of PET and MR images. It was demonstrated that incorporation of the anatomical information using this approach, following parameter optimization, produces significant improvement in the noise versus bias tradeoff in ROI-based quantitative analysis compared with conventional MAP reconstruction.

MRI-guided partial-volume correction in PET/MRI

The accuracy of PET for measuring regional radiotracer concentrations is limited by the finite spatial resolution capability of current-generation clinical PET scanners and the resulting partial-volume effect (PVE). Accurate PET quantification requires that the source size be greater than two to three times the scanner's spatial resolution, expressed in terms of

full-width at half-maximum. Any object with smaller dimensions only partly occupies this characteristic volume, such that acquired counts are spread over a larger volume owing to the limited spatial resolution of the PET scanner. Under these circumstances, corresponding PET images still reproduce the total amount of radiotracer uptake within an object but do not represent the regional activity distribution within this volume. A number of strategies have been proposed to correct for PVE [60]. The most straightforward approach uses recovery coefficients, which can be determined through experimental studies involving the use of spheres of different sizes. This simple approach produces acceptable results for objects with similar shape as the calibration phantom used for derivation of recovery coefficients (e.g., tumors of spherical shape). More refined approaches rely on anatomically guided postreconstruction techniques, in which the size and shape of corresponding objects assessed by structural imaging (MRI or CT) [61] are used instead to correct for this effect.

The PVE is among the major concerns in brain PET imaging in connection with quantification of cerebral metabolism in the atrophied brain, such as with Alzheimer's disease. Various voxel-based MRI-guided PVE correction methods have been proposed. The most popular technique consists of segmenting MR images into white and gray matter after PET/MRI registration. This is followed by convolving the segmented white and gray matter images by a Gaussian point spread function representing the PET scanner's spatial resolution. The PVE-corrected gray matter PET image is achieved by subtracting the convolved PET white matter image from the original PET image, followed by division by the convolved gray matter MR image. The final step involves the application of a binary mask to the gray matter region [62].

The overall accuracy achieved by MRI-guided PVE correction in PET depends upon the accuracy achieved by each procedural step, including image registration and MRI segmentation. This has been investigated in detail for the voxel-based approach [61]. The high soft-tissue contrast provided by MRI provides reasonable accuracy in terms of differentiation between gray and white matter. Nevertheless, errors in segmentation of brain tissue components have been found to be of greater significance [63]. For instance, a 25% error in total volume produces a 5% decrease in the caudate nucleus apparent recovery coefficient [64]. It is interesting to note that the effect of segmentation error is limited to the missegmented region. Inaccuracies from segmentation can be regarded in the framework of a more broad question of tissue heterogeneity. In fact, the main limiting feature of these algorithms is the assumption regarding the homogeneity of radiotracer distribution in each region or tissue component. Overall, it appears that the success of MRI segmentation has a higher impact on the accuracy of the corrected estimates [63] compared with the influence of image registration, although some studies seem to suggest that registration errors have the greatest impact on data accuracy and precision [61].

More refined strategies using multiresolution synergetic approaches merging anatomical and functional information seem to have the potential to overcome the limitations of classical techniques. However, their feasibility in a clinical setting still needs to be demonstrated [65]. PVE correction can also be included directly into statistical reconstruction algorithms through the use of an appropriate mathematical formulation of PVE in the forward model along with other physical degrading factors governing the physics of PET [58].

MRI-guided motion compensation in PET/MRI

Recent advances in PET instrumentation have made it possible to achieve high spatial resolution, which motivates further development and clinical implementation of sophisticated motion correction strategies. The various sources of motion, including unwanted patient motion, cardiac motion, and respiratory motion, and correction strategies specifically developed to reduce or eliminate them have been reviewed recently [66]. Overall, three broad approaches were reported in the literature: 1) nonrigid registration of independently reconstructed images; 2) initial estimation of motion information from gated PET or MR/CT images, subsequently used in a new reconstruction applied to all gated frames; and 3) simultaneous estimation of motion parameters and images.

Motion between or during anatomical/molecular data acquisition remains an important challenge for PET/MRI protocols. The characteristic misalignment between PET and CT images at the level of the diaphragm in PET/CT systems resulting from breathing pattern differences is expected to be partly addressed by PET/MRI owing to the longer acquisition time of MRI sequences used for attenuation correction, which results in temporal averaging that would improve PET and MRI registration in some situations. In addition, the use of a specific respiratory protocol in PET/MRI can improve the spatial correspondence between PET and MRI. Owing to the typical duration of PET data acquisition (2–3 minutes/bed position), a PET image corresponds to an average of several respiratory cycles and is susceptible to motion-related distortion. Similarly, typical low-resolution MR images suitable for attenuation correction involve averages over multiple respiratory cycles, although the averaging process in MRI is different from that in PET. More importantly, severe motion artifacts may appear when there is marked organ motion with increased noise and smaller-appearing organ size on the MRI attenuation map, with subsequent bias in the attenuation correction procedure. Ideally, PET and MR images should correspond to the same phase of the respiratory cycle and be matched to achieve accurate attenuation correction and improved spatial resolution. To achieve good matching between PET and MR images at a specific respiratory phase, the patient's breathing during scanning should be synchronized to reduce distortional effects of respiratory motion. Provision of breathing instructions to patients prior to scanning may also be useful.

An assortment of MRI motion-tracking methods predominantly for rigid-body motion have been employed in the clinical setting, including, but not limited to, embedded cloverleaf navigators [67]. One such technique uses motion estimates derived from high temporal resolution MRI during simultaneous

acquisition of structural or functional MRI data for motion correction of corresponding brain PET data, demonstrating that MRI-derived motion can be used to improve PET image quality, thus increasing confidence in interpretation, reproducibility, and quantitative accuracy [68].

Current trends focus on four-dimensional MR-derived motion correction strategies to reduce artifacts observed in PET/CT by developing MRI-guided motion-compensated PET attenuation correction schemes, and research efforts should focus on designing suitable protocols to minimize MRI artifacts while also reducing mismatch between MR and PET images. Motion-free PET images are obtained by correcting motion-related blurring through MRI-derived motion estimates, allowing for improved image quality and accurate quantification of PET data compared with correction using PET-only motion information. Concurrent PET/MRI can also enable potential nonrigid motion compensation in whole-body PET imaging without increasing acquisition time [69]. Furthermore, three-dimensional cine MRI sequences for tracking the position and deformation of organs can be used to derive deformation fields for incorporation into statistical PET image reconstruction algorithms, although this approach can be complex [70], [71].

The use of tagged MRI for motion tracking in the phase domain to derive motion estimates in deformable registration during concurrent PET/MRI data acquisition was recently reported [72]. The conventional harmonic phase tracking technique is regularized, and the derived motion fields are incorporated in the system matrix of a statistical PET reconstruction algorithm. Preliminary results using computer simulations and a deformable phantom appear promising. Further investigation reported in more recent studies demonstrated the full potential of MRI-guided motion correction and its feasibility in clinical and research settings [73]–[75].

Clinical applications of PET/MRI

Hybrid whole-body human PET/MRI systems have been available since 2010; however, despite the initial excitement, the implementation of these systems in a clinical environment is still in an early phase. Among all potential clinical PET/MRI applications, recent advances in adult and pediatric oncology emerge as the most promising application fields. So far, only very few studies based on relatively small sample sizes have addressed the clinical workflow, feasibility, and optimized PET/MRI protocols in oncology [76]–[78]. Although some authors report no added diagnostic benefit in comparison with PET/CT or MRI [76], [79], [80], [81], others describe added value in selected cases [82]–[84]. During the past two years, there has been only a slow increase in the rate of new PET/MRI system installations, mainly owing to lack of clearly defined applications, and currently, there is little evidence to validate key applications based on the experience of multiple centers. This lack of significant progress can probably be explained by the fact that both MRI and PET/CT are powerful methods that are already well implemented in everyday clinical oncology.

Clinical workflow and protocols

A particular problem hampering the clinical implementation of PET/MRI in oncology is the lack of standardized imaging protocols and workflows because large variations in MRI protocols, sequences, and image requirements exist. Currently, most PET/MRI examinations in oncology are obtained using multistep protocols, which are very similar in design to PET/CT protocols. PET/CT protocols include a total-body low-dose CT, followed by a PET acquisition. In some institutions, contrast-enhanced CT is additionally obtained to avoid false-negative or false-positive PET readings, thereby improving the overall diagnostic yield [85]. In analogy to PET/CT, PET/MRI examinations can be performed by obtaining a rapid total-body MRI sequence for attenuation correction and localization of focal uptake, which is then followed by a whole-body PET. Although this approach is time-effective regardless of scanner type (simultaneous or sequential), the approach is not optimal for pretherapeutic tumor staging because it provides neither detailed anatomical nor functional MRI information.

The second PET/MRI approach consists of a rapid total-body PET/MRI acquisition and an additional high-resolution MRI examination of anatomical ROIs depending on the clinical situation. In simultaneous systems, this full diagnostic MRI (anatomical, diffusion-weighted, and perfusion sequences) can be performed during the PET acquisition, whereas in sequential systems, it is usually performed during the 60 minutes necessary for tracer uptake and prior to PET acquisition. However, not all MRI sequences can be acquired during the PET acquisition even in simultaneous scanners, and the total PET/MRI in-room time may be quite long (60–90 minutes), with most of the time being allotted to the MRI acquisition [77], [86], [87]. Therefore, in practical terms, the length of the MRI acquisition is a major limiting factor in the clinical implementation of PET/MRI in everyday routine provided that full use of multiparametric MRI capabilities is sought.

To compete with PET/CT acquisitions, which usually take around 30–40 minutes, some authors [31], [93] have suggested limiting the number of MRI sequences to the absolute minimum necessary for the oncologic diagnosis. However, there is no consensus today on the essential sequences necessary for tumor imaging, and different investigators have proposed different protocols. These are based not only on institutional preferences and technical parameters specific to different vendors but also on ongoing research protocols, time-effectiveness issues, cost, and—last but not least—the type of tumor to be imaged [76], [77], [88]. For example, there is increasing evidence supporting the utility of routinely obtaining diffusion-weighted imaging (DWI) in head and neck cancer and lymphoma. Whole-body MRI with DWI has a high sensitivity (96–97%) in the detection of lymphoma [89]. Gu et al. [89] evaluated whole-body MRI without and with DWI in the detection of known ^{18}F-Fluorodeoxyglucose (^{18}F-FDG)-avid lymphomas in 17 adult patients. By adding DWI to anatomical MRI, sensitivity was increased from 89% to 97% ($p = 0.002$); in particular, the accuracy for detecting nodal and extranodal disease in the abdomen and pelvis was improved, but without

affecting overall staging. Lin et al. [90] suggested that whole-body DWI may help to identify additional lymphoma lesions relative to the lesions already identified by ^{18}F-FDG PET/CT, whereas Punwani et al. [91] reported the complementary value of DWI to ^{18}F-FDG PET for prediction of site-specific interim response to chemotherapy, thereby supporting the need to incorporate DWI sequences into integrated PET/MRI protocols for lymphoma. In a similar fashion, Varoquaux et al. [92] showed that, although DWI and FDG PET may both reflect increased cell proliferation in head and neck squamous cell carcinoma, the two modalities refer to different biological phenomena, and their respective metrics, apparent diffusion coefficient (ADC) and SUV, are independent biomarkers, thereby having the potential to provide complementary information (Figures 6 and 7). The same authors showed that measurements of ADC and SUV values are reproducible with almost perfect interobserver and intraobserver agreements for both methods, and they observed a trend toward higher SUV and lower ADC values in poorly differentiated head and neck cancers compared to their well-differentiated or moderately differentiated counterparts [92].

In an attempt to reduce the total number of MRI sequences, some investigators have questioned the use of contrast-enhanced MRI sequences [93]. However, in head and neck squamous cell carcinoma, contrast-enhanced MRI sequences are superior to CT and PET/CT for a variety of findings that are essential for the therapeutic choice, such as invasion of the skull base, perineural spread, and retropharyngeal lymph nodes or detection of extranodal spread in metastatic lymph nodes [86]. In addition, the combination of contrast-enhanced T1-weighted and T2-weighted sequences allows more precise differentiation between tumor and peritumoral inflammation, and it appears that the differentiation between these two conditions on the basis of MRI signal intensity characteristics can have direct implications on patient outcome after radiation therapy [86]. Morphologic MRI also appears to provide a higher accuracy than FDG PET/CT in detecting residual and/or recurrent nasopharyngeal carcinoma, and the combination of PET/CT and MRI seems to be superior to either modality alone for the detection and precise locoregional evaluation of recurrent disease [94]. In other tumor types, such as in breast cancer, the use of contrast-enhanced MRI sequences is essential. As shown by Taneja et al. [81], the morphologic MRI appearance of a breast lesion (size, shape, and pattern of enhancement) and its time–signal intensity curve after intravenous contrast material (progressive, plateau, or washout) yield

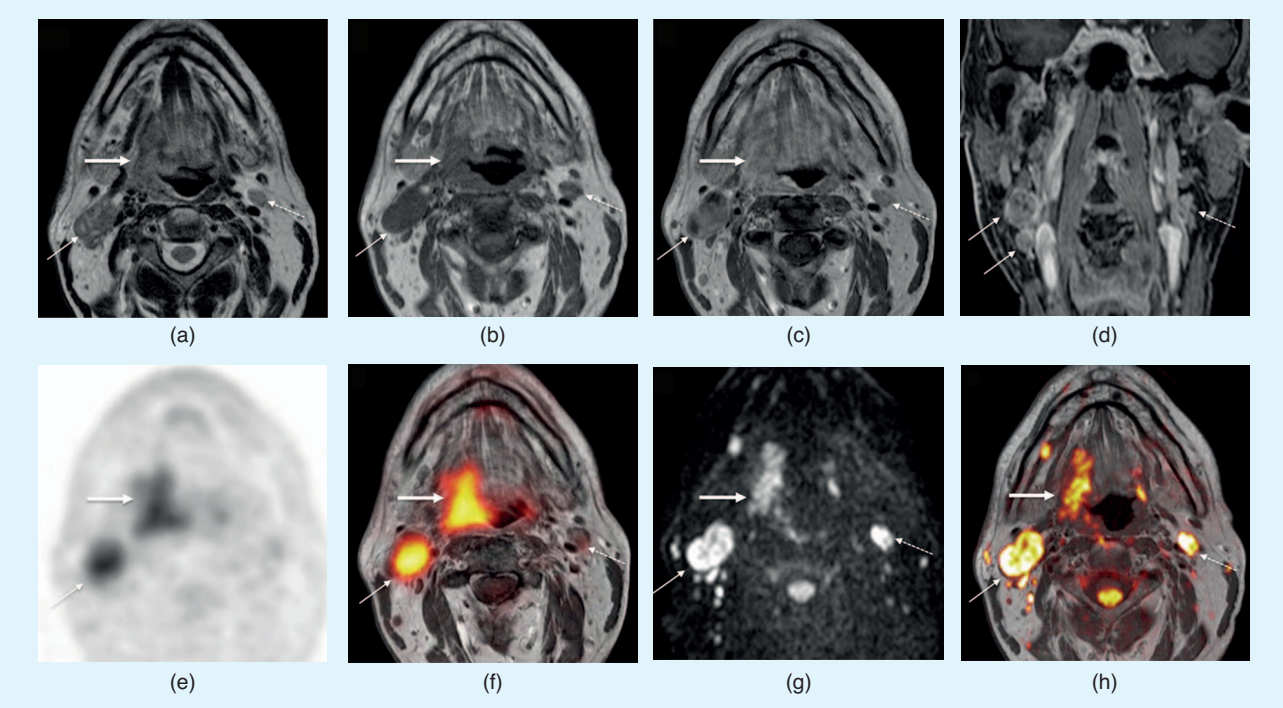

FIGURE 6. Multiparametric PET/MRI in head and neck squamous cell carcinoma. Complementary values of DWI, PET, and contrast-enhanced images: (a) Axial T2, (b) T1, (c) contrast-enhanced T1, (d) coronal contrast-enhanced fat-saturated T1, (e) axial PET, (f) fused PET with contrast-enhanced T1, (g) axial b1000 image from DWI, and (h) fused b1000 with contrast-enhanced T1. Right tonsillar cancer (thick arrows) invading the base of the tongue and posterior oropharyngeal wall and two right level 2 lymph node metastases are shown [thin arrows in (a)–(d)]. (c) Contrast-enhanced T1 reveals nodal necrosis, and (d) the corresponding fat-saturated T1 with gadolinium shows extranodal spread particularly well [spiculated margins in (d), thin arrows] not revealed by (a) and (b). (e) and (f) show high FDG uptake in the tumor ($SUV_{max} = 9.2$) and, on the right, level 2 lymph nodes ($SUV_{max} = 7.5$). (g) and (h) show restricted diffusivity in the tumor (mean ADC $= 1.0 \times 10^{-3}$ mm^2/second) and in the ipsilateral lymph nodes (mean ADC $= 1.16 \times 10^{-3}$ mm^2/second). These findings were confirmed histologically. A contralateral 8-mm large level 2 lymph node (dashed arrows) with restricted diffusivity (ADC $=1.08 \times 10^{-3}$ mm^2/second) is seen in (g) and (h). Based on DWI, this left level 2 lymph node is considered suspicious for metastasis, although the FDG uptake and the morphologic aspect instead suggest a benign lymph node. Histology revealed moderately differentiated squamous cell carcinoma of the tonsil with bilateral lymph node metastases.

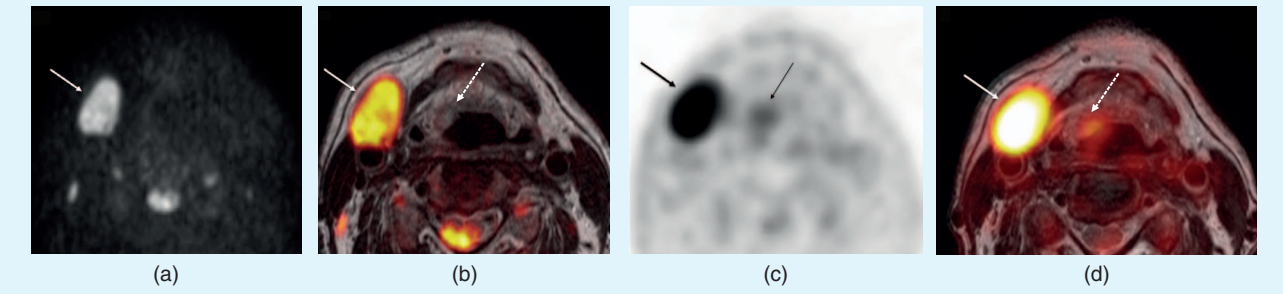

FIGURE 7. The detection of an unknown primary tumor with PET/MRI in a 60-year-old patient with nodal metastasis from squamous cell carcinoma. Endoscopy performed prior to PET/MR did not reveal a primary tumor. (a) b1000 image from DWI and (b) fused b1000 with T2-weighted image show a large level 2 lymph node metastasis (thick arrows) but no clearly identifiable primary tumor with restricted diffusivity. (c) A corresponding PET image and (d) fused PET with T2-weighted image confirm the metastatic node (thick arrows) and also reveal a small suspicious area located in the right pre-epiglottic space (thin dashed arrows). A repeat deep biopsy showed poorly differentiated squamous cell carcinoma located beneath an intact mucosa of the right epiglottis. Retrospectively, a small nodule can be seen on the T2-weighted image (dashed arrow).

a higher sensitivity for the detection of breast cancers than ^{18}F-FDG PET. Therefore, PET/MR in breast cancer staging cannot be performed without contrast material in particular because breast lesions and metastatic axillary nodes may be ^{18}F-FDG–negative. Punwani et al. [95] have shown the indispensable role of dynamic contrast-enhanced MRI in Hodgkin lymphoma staging to detect splenic involvement. There are many other examples in which contrast-enhanced sequences are indispensable in the oncologic context, a detailed description being beyond the scope of this article. It therefore appears that contrast-enhanced sequences cannot be excluded from the MRI protocol in most oncologic situations without compromising MRI performance. Nevertheless, standardized PET/MRI protocols and harmonized data acquisition across multiple institutions are desirable. As suggested at the Third International Symposium on PET/MRI [87], an alternative to institutional series would be to create a PET/MRI registry for pooling data from multiple centers. Such a registry would facilitate evaluation of clinical data in terms of diagnostic performance and would equally expedite the evaluation of the impact of PET/MRI on patient management [87].

Finally, the third PET/MRI approach is to perform a total-body, full diagnostic, high-resolution MRI in addition to the total-body PET acquisition. Currently, this option cannot be implemented in clinical settings owing to the unacceptably long in-room time.

Feasibility studies and PET image quality in PET/MRI versus PET/CT

Several studies have shown that PET/MRI is feasible with both simultaneous and sequential systems in patients with a variety of tumors, including lung cancer, breast cancer, brain tumors, head and neck cancers, and pediatric tumors [76]–[78], [80], [88], [96]. A few authors [76], [78], [79], [93], [96] have compared PET/MRI results with PET/CT results, with all patients undergoing a single dose injection of ^{18}F-FDG. Although some authors [78], [79] first performed PET/CT and immediately thereafter PET/MRI, others chose to perform PET/MRI first and then PET/CT. Experienced observers, who were blinded to clinical data, evaluated the PET/CT and PET/MRI data sets. Despite variable protocols, in all studies, PET/MR image quality, fusion quality, lesion conspicuity, and anatomical lesion localization were good to excellent, and no statistically significant difference was found between the rating scores for image quality, fusion quality, lesion conspicuity, and anatomical localization, as well as with respect to the number of detected focal uptake lesions in PET/MRI and PET/CT, respectively [76], [78], [79], [96].

In terms of quantification, all authors reported a high correlation for SUV values measured in PET/MRI and PET/CT for organs and for malignant and benign focal uptake [76], [78], [79]. However, several investigators have reported that SUVs for focal uptake and normal organs may be underestimated by 11–20% in PET/MRI compared with PET/CT; this observed underestimation results in a limited concordance of SUV measurements between the two modalities [76], [78], [79]. In summary, although quantification issues are not yet completely solved, as discussed in the section on quantitative PET/MRI, several studies have shown that for the detection and localization of FDG-avid lesions and for differentiating between benign and malignant lesions in pediatric and adult patients, PET/MRI results are comparable with PET/CT results. In other words, from the clinical point of view, lesion detection and characterization with PET/MRI do not appear to be significantly affected by limitations in quantitative accuracy. In a clinical setting, the significantly lower radiation exposure when using PET/MRI compared with PET/CT constitutes an important benefit, especially for serial studies and in the pediatric population.

Pitfalls and artifacts

Several artifacts may hamper the interpretation of PET/MRI examinations. They are caused mainly by PET/MRI hardware, MRI and PET physics, physiologic phenomena, the presence

of medical devices, and MRI contrast agents [97]. Artifacts related to the technical aspects and conceptual design of PET/MRI systems can be caused by the presence of RF coils in the FOV and may result in additional attenuation and scatter with more complex patterns. Because the position of RF coils is not visualized on MR images, integrated systems use fixed coils at known positions and do not commonly correct for surface coils (which have a negligible effect), whereas sequential systems use "coil identification scans" to account for the attenuation of RF coils.

Truncation artifacts can be observed in both PET/CT and PET/MRI and typically occur in large patients scanned with arms down. In PET/MRI, they are caused by the fact that the transaxial FOV of the MRI acquisition (~45 cm) is smaller than the FOV of the PET acquisition (~70 cm). Inhomogeneity of the static magnetic field (B0) and gradient field nonlinearity at the FOV periphery are additional factors predisposing to truncation artifacts. Because parts of the body are outside the FOV of the MRI scan, the resulting attenuation map is incomplete, thereby leading to visible artifacts on the corresponding PET images and underestimation of SUV values. Truncation artifacts can be corrected by obtaining a compensated attenuation map from nonattenuation-corrected emission PET data, which is then fused with the truncated map [98], or through more advanced approaches, such as the MLAA algorithm described in the previous section.

Fold-over artifacts occur along the phase-encoding direction if the chosen FOV of the MRI acquisition is smaller than the part of the body that needs to be imaged. Fold-over artifacts may lead to incorrect PET quantification but can be easily corrected by changing the direction of phase encoding. However, this approach results in a prolonged MRI acquisition time.

Pulsation artifacts occur along the MRI phase-encoding direction and are often seen in the chest, head and neck area, or upper abdomen. They are the consequence of vascular and cardiac pulsation or turbulent flow and may lead to erroneous quantification of tracer uptake mainly in lymph nodes located along vascular structures. Possible solutions to correct pulsation artifacts include changing the phase-encoding direction or applying flow compensation techniques.

Local destructive interferences, eddy currents and standing-wave effects, which are more common at 3 T than at 1.5 T, can lead to signal loss in the area of interest, thereby impairing PET/MRI interpretation. Eddy currents and standing-wave artifacts may occur in the upper abdomen of overweight patients or in patients with peritoneal fluid. Potential solutions include the use of parallel RF coil technology and placing cushions with an ionic solution on the abdomen [99].

A recently described effect observed in simultaneous PET/MRI systems is the shine-through artifact [7]. As reported by Kolb et al. [7], the static magnetic field (B0) of the MRI scanner affects the trajectory of positrons by reducing the positron range in the plane perpendicular to B0 (axial plane) and by elongating the positron range along the direction of B0 (craniocaudal direction). In PET/MRI, the shine-through artifact can be seen with low-energy PET radionuclides only if the area of high tracer uptake is in the immediate vicinity of an air cavity, a situation typically observed in the head and neck region. Depending on the orientation of the larynx and trachea in the magnetic field, the magnitude of the artifact may vary considerably. It results in an elongated shape of tracer uptake on coronal and sagittal images and in an apparently increased tracer concentration diametrically opposed to the location of the actual lesion. The shine-through artifact can potentially lead to overestimation of tumor involvement in PET/MRI [7]. Adequate compensation techniques for this artifact are not yet available.

Bulk and respiratory motion-induced mismatch between MRI and PET data acquisition in sequential scanning can result in misregistration. Misregistration can hinder precise tumor localization in small-sized lesions and, in severe cases, overall image interpretation. To avoid this pitfall, anatomical MRI sequences need to be carefully analyzed, and interpretation of PET findings should always take morphology into account. Motion artifacts have been reported mainly in head and neck cancer patients and pediatric oncology patients. Motion artifacts are caused by patient stress from long scanning times, dyspnea, or pain. Careful patient instruction, breaks between sequences, or pain medication, whenever necessary, can significantly reduce the number of poor-quality images caused by motion. Diaphragmatic excursion during respiration may affect interpretation of the basal lung, liver, pancreas, and spleen. PET images in both PET/CT and PET/MR tend to be blurred, the effective resolution above and below the diaphragm is diminished, and tracer uptake may be underestimated. To avoid misalignment, several authors recommended acquiring the MRI attenuation correction sequence and the anatomical reference sequences during shallow free-breathing or in end-expiratory breath hold [97], [100]. Current developments in PET/MRI utilizing motion-sensitive MRI pulse sequences, such as velocity-encoded phase-contrast MRI and tagged MRI, have the potential to outperform PET/CT, for which similar correction strategies do not exist [99], [101].

Although these methods improve PET image quality, they require a modification of the PET/MRI protocol. Recently, Manber et al. [102] showed that a respiratory signal could be extracted from raw PET list-mode data, thus substantially improving clinical PET image quality only by adding an additional 1-minute dynamic MR scan.

A particular problem encountered in pelvic PET/MRI is the misalignment of the bladder owing to the continuous physiologic secretion of urine and resulting bladder volume change during the procedure. This problem is encountered mainly when patients are imaged with sequential PET/MRI systems. Several practical solutions have been proposed, including obtaining an additional fast MRI sequence for image fusion with PET just before starting the PET acquisition, restricting water intake 4 hours before the exam, and asking the patient to void just before beginning the image acquisition [77].

Susceptibility artifacts around ferromagnetic objects, typically dental restorations or osteosynthesis material, result in

distortion of the surrounding anatomy and in bright and dark areas on all sequences, but most frequently on gradient echo sequences, DWI sequences, and fat-saturated sequences. Geometric distortion is a well-recognized problem inherent to DWI sequences; it is caused by B0 susceptibility differences. Geometric distortion of DWI images is a common cause of misregistration of anatomical and b1000 images. In addition to the effects on image quality, susceptibility artifacts caused by ferromagnetic objects can have an impact on the attenuation coefficient on the MRI-based or CT-based attenuation map. In consequence, artifacts caused by dental implants, hip prostheses, sternal wires, metallic port catheter systems, or other metallic implants can affect SUVs measured in PET/MRI and PET/CT. In PET/MRI, metallic implants result in an apparently decreased focal uptake. A priori knowledge of these pitfalls avoids erroneous image interpretation. Nevertheless, artifacts caused by metallic implants are, in general, larger and more disturbing on CT and PET/CT than on MRI and PET/MRI (Figure 8). Strategies to reduce metal artifacts in PET/MRI are quite challenging, and up until now, this area is still a work in progress. New sequences, such as slice encoding for metal artifact correction with view angle tilting, have been developed for standalone MRI systems; however, they have not yet been tested in hybrid PET/MRI systems [103]. A different approach for metal artifact correction in PET/MRI has been proposed by Ladefoged et al. [104], who developed an automatic algorithm for correction of dental artifacts in PET/MRI by first using a template of artifact regions and then representing the artifactual regions with a combination of active shape models and *k*-nearest neighbors.

Last but not least, MRI contrast agents, such as iron oxide nanoparticles, which are used mainly to detect focal hepatocellular lesions, may hamper the interpretation of PET/MRI studies. The main effect of iron oxide nanoparticles is on T2* relaxation; they cause signal loss in T2*-weighted and T2-weighted images owing to the susceptibility effects of the iron oxide core. In the liver, the particles accumulate in the Kupffer cells of the normal reticuloendothelial system while sparing lesions lacking Kupffer cells, such as metastases. Because this effect may last for several weeks, it may affect MRI attenuation maps and should be considered when interpreting PET/MRI examinations, although some studies reported negligible quantification bias because MRI contrast agents have almost the same linear attenuation coefficient as water [105].

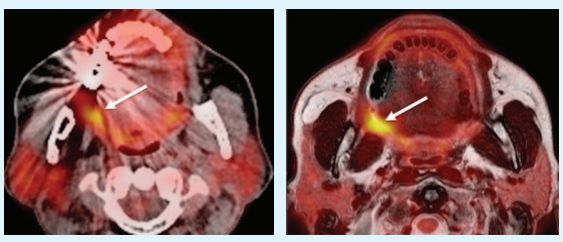

FIGURE 8. Dental artifacts affect PET/MRI less than PET/CT. (a) A PET/CT image shows major streak artifacts from dental implants hampering image interpretation. Note the poorly delineated area of higher FDG uptake on the right (arrow). (b) A corresponding hybrid PET/MRI (PET fused with axial T2-weighted image) image obtained from the same patient clearly shows an FDG-avid tumor in the right anterior tonsillar pillar (arrow) extending into the retromolar trigone. The biopsy revealed squamous cell carcinoma.

Clinical data on diagnostic accuracy of PET/MRI in oncology

Very little data are currently available regarding the diagnostic performance of hybrid PET/MRI systems in oncology. This fact is due to the difficulty in obtaining a rigorous standard of reference based on histology and/or long-term follow-up. In most published studies, PET/CT is used as the standard of reference, whereas one could argue that false-positive and false-negative readings may equally occur with this modality. From a clinical perspective, some incremental progress has been reported over the past two years in breast cancer [81], pediatric oncology [96], prostate cancer [82], head and neck chondrosarcoma [83], and neck irradiation [106], whereas no added value compared with other imaging modalities (PET/CT or MRI) could be demonstrated for lung cancer [107], detection of lung nodules [108], and nodal staging in head and neck squamous cell carcinoma [80].

Taneja et al. [81] assessed the utility of whole-body ^{18}F-FDG PET/MRI in the initial staging of breast cancer in 36 patients with histologically confirmed invasive ductal carcinoma. Primary lesions, lymph nodes, and distant metastases were evaluated with PET, MRI, and PET/MRI for lesion count and diagnostic confidence (DC). The study yielded the highest DC score of 5 with PET/MRI compared with PET (median DC score = 4) and MRI (median DC score = 4) alone. MRI detected 47 satellite lesions, of which only 23 (49%) were FDG-avid with multifocality and multicentricity in 21 (58%) patients. The study equally showed sensitivities of 60 and 93% for PET and MRI, respectively, in the detection of axillary lymph nodes, with a specificity of 91% for both. Combined PET/MRI increased the DC for nodal involvement. Ninety-one metastatic lesions were detected in PET (DC ≥ 4) and 105 in MRI (DC ≥ 4), with the difference being statistically significant ($p = 0.001$). The authors concluded that PET/MRI is useful as an initial staging modality in breast cancer patients because the DC is higher with PET/MRI compared with PET or MRI alone; however, no statistical comparison was performed to evaluate the added value of PET/MRI compared with MRI alone [81]. In particular, on the basis of the published figures, the authors reported a similar sensitivity and staging accuracy with MRI and PET/MRI [81].

Regarding pediatric oncology, several studies have shown that PET/MRI is technically feasible in children as young as six years old without general anesthesia, as well as in adolescents, showing adequate quantitative accuracy with SUVs compared with those obtained in PET/CT [96]. Schäfer et al. [96] demonstrated that PET/MRI achieved equivalent lesion detection rates compared with PET/CT, with the former offering

markedly reduced radiation exposure. Currently, reported effective radiation doses for PET/CT are in the range of 25 mSv, whereas for PET/MRI, they are in the range of 7 mSv [87]. Child-specific patient preparation procedures are, however, mandatory to obtain good-quality PET/MRI examinations. Among whole-body PET/MRI applications identified in pediatric oncology, staging of Hodgkin lymphoma with DWI and dynamic contrast-enhanced MRI sequences has been identified as promising because PET/MRI can enhance the accuracy of lesion detection compared with PET/CT [91]. Data on other pediatric tumors, such as sarcomas and neuroblastomas, are not yet available.

As opposed to the high signal intensity of the peripheral zone, prostate cancers typically display a low signal on T2-weighted images. However, tumors arising from the transitional zone are often difficult to detect owing to the heterogeneous T2 appearance of the transitional zone, with this mixed signal being often caused by benign hyperplasia. Therefore, it has been suggested that a multiparametric imaging approach including T2-weighted sequences, DWI, dynamic contrast-enhanced imaging, and ^{18}F-choline PET may improve pretherapeutic diagnostic accuracy. In a recent publication based on a series of 24 patients with total prostatectomy, de Perrot et al. [82] demonstrated that ^{18}F-choline PET/MRI had an improved diagnostic accuracy in the peripheral zone compared with multiparametric MRI but had no added value in the transition zone owing to adenomatous hyperplasia. ADC and SUV_{max} were not correlated biomarkers, suggesting that they may provide complementary information in the workup of these tumors [82].

Chondrosarcoma of the larynx is a rare, low-grade malignancy; in a minority of cases, a dedifferentiated component can occur within a chondrosarcoma. Histologically, a well-differentiated cartilaginous component is juxtaposed to the dedifferentiated component, with an abrupt transition between the two tissue types [83]. Purohit et al. [83] reported that the diagnosis of dedifferentiation can be suggested in PET/MRI owing to the morphologic and metabolic findings because the well-differentiated component has a low signal on T1-weighted images, slight peripheral enhancement, a high signal on T2-weighted images, high ADC values, and low SUVs, whereas the dedifferentiated component has a low signal on T1-weighted images, major inhomogeneous enhancement, a moderately high signal on T2-weighted images, low ADC values, and high SUVs. The authors therefore concluded that PET/MRI can provide additional functional information to supplement the morphologic mapping and histopathology of these tumors [83].

^{18}F-FDG PET/CT is widely accepted as the evaluation method of choice for staging nonsmall cell lung cancer (NSCLC). Heusch et al. [107] compared a dedicated pulmonary ^{18}F-FDG PET/MRI protocol with PET/CT for primary and locoregional lymph node staging in NSCLC patients using histopathology as the standard of reference. The results from PET/MRI and PET/CT agreed on T stages in all 16 patients (100%). There was no statistically significant difference between PET/CT and PET/MRI regarding detection of lymph node metastases ($p = 0.48$) and SUV measurements, and tumor size measurements derived from PET/CT and PET/MRI showed a high correlation. The authors concluded that compared with ^{18}F-FDG PET/CT, PET/MRI with a dedicated pulmonary MRI protocol does not provide advantages in thoracic staging in NSCLC patients [107].

Most investigators currently consider multidetector CT (MDCT) the imaging modality of choice for the detection of pulmonary nodules. Although MDCT has high sensitivity in the detection of pulmonary nodules, its capability to differentiate between benign and malignant nodules in patients with primary malignancy is limited [108]. Discrimination between malignant and benign nodules is, however, facilitated by the use of ^{18}F-FDG PET/CT. One of the major potential disadvantages of PET/MRI over PET/CT is the lower sensitivity of MRI compared with CT in the detection of small pulmonary nodules. Chandarana et al. [108] compared the performance of PET, MRI, and combined PET/MRI in the detection of lung nodules in oncologic patients with clinically indicated PET/CT. PET/CT was considered the standard of reference. The combination of PET and MRI acquired using a hybrid PET/MRI system with a radial T1-weighted gradient echo sequence had a higher sensitivity for lung nodules compared with PET or MRI alone. The sensitivities of PET/MRI were 70, 96, and 23% for all nodules together, FDG-avid nodules, and non-FDG-avid nodules, respectively. When nodule size was analyzed, PET/MRI had a sensitivity of 89% for the detection of nodules with a diameter of at least 5 mm and a sensitivity of 38% for the detection of lesions smaller than 5 mm. The authors therefore concluded that PET/MRI has a high sensitivity for FDG-avid lung nodules and for nodules 5 mm or larger in diameter but a lower sensitivity for small non-FDG-avid nodules [108]. Results from our institution [86] confirm these findings and show that although the conspicuity of lung lesions may be less clear in PET/MRI compared with PET/CT, FDG-avid lung nodules and nodules larger than 5 mm are equally well detected with both modalities (Figure 9).

In a prospective study including 38 patients with squamous cell carcinoma of the head and neck, Platzek et al. [80] evaluated the performance of PET, MRI, and PET/MRI in the detection of lymph node metastases. Results were compared on the basis of receiver operating characteristic analysis, whereas histology served as the standard of reference. Metastatic nodes were present in 42% of the 38 patients and in 10% of the 391 dissected lymph node levels. There were no significant differences among PET/MRI, MRI, and PET ($p > 0.05$) regarding accuracy for cervical metastatic disease. The authors therefore concluded that in head and neck cancer, FDG PET/MRI does not significantly improve accuracy for cervical lymph node metastases compared with MRI or PET [80]. Nevertheless, it is important to mention that MRI did not include DWI acquisitions in this study.

The variable appearance of recurrent tumors after radiation therapy of the head and neck and treatment-induced expected tissue alterations and complications often render MRI or

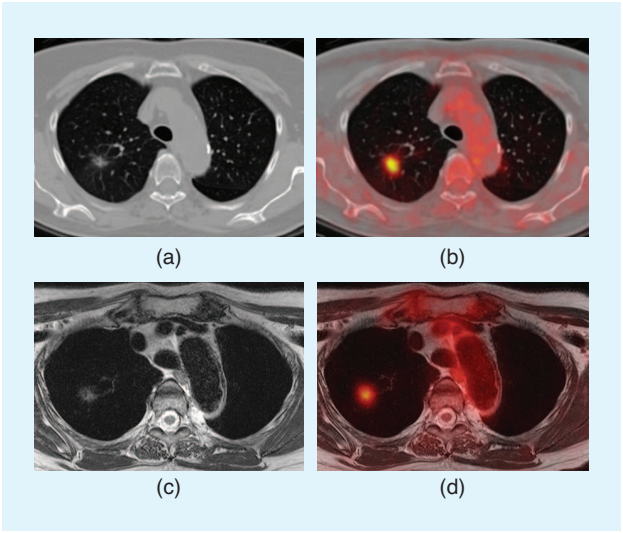

FIGURE 9. The detection of larger FDG-avid pulmonary nodules with PET/MRI and PET/CT. This patient was a follow-up case of a salivary gland adenocarcinoma. (a) and (b) Axial PET/CT and (c) and (d) corresponding PET/MR images obtained within 1 hour and after a single-dose injection of FDG show a spiculated 10 × 9 × 9-mm large lung nodule with a central cavitary area in the upper right lobe and with focal FDG uptake (SUV_{max} PET/CT = 3.9, SUV_{max} PET/MR = 4.8), suggesting either metastatic disease or a synchronous second primary tumor. A biopsy revealed a second primary pulmonary squamous cell carcinoma.

PET/CT image interpretation very demanding. As reported by Varoquaux et al. [106], PET/MRI with DWI holds promise to facilitate differentiation between tumor recurrence and radiation-induced changes and complications. In particular, multiparametric imaging, including anatomical, contrast-enhanced, DWI, and PET information, can be very beneficial in solving diagnostic dilemmas. In their recent article on DWI/MRI and PET/MRI of the irradiated neck, the authors provided a comprehensive approach to the understanding of key features of radiation-induced edema, fibrosis and scar tissue, soft-tissue necrosis, osteochondronecrosis, brain necrosis, and thyroid disorders by discussing the complementary role of DWI/MRI and PET/MRI in these entities and in the detection of recurrent disease. The authors concluded that multiparametric PET/MRI leads to a major reduction of interpretation pitfalls, thereby increasing the DC in interpreting examinations of the irradiated neck [106].

Diagnostic challenges related to multiparametric imaging

Interpreting hybrid PET/MRI studies with multiparametric data sets can be quite challenging in clinical routine owing to the huge amount of complex information and the difficulty taking all measured parameters into consideration. Current research protocols based on multiparametric data acquisitions already use classification algorithms in the analysis of PET/MRI data, including algorithms based on Gaussian distribution models or support vector machine analysis. Within the same tumor, these classification algorithms can separate tissue regions on the basis of their different PET, ADC, or perfusion maps, therefore enabling more accurate differentiation between areas of increased proliferation, apoptosis, fibrosis, and viable cells. Differentiating between these entities may have a tremendous impact on future radiotherapy regimens in view of tailored treatment options.

A practical problem that has not yet been solved is how to deal with discrepant multiparametric data from PET/MRI during everyday image interpretation. Should one rely on the morphologic and perfusion information or on the PET or DWI information? How should one weight the value of each parameter to increase the diagnostic yield and avoid unnecessary biopsy? Certainly, the clinical experience of the radiologists and nuclear medicine physicians interpreting the data plays a major role, and the interdisciplinary collaboration with oncologists, surgeons, pathologists, and radiation oncologists for a meaningful integration of all imaging and biological patient data is crucial. Although recent publications on the clinical value of multiparametric PET/MRI show promising results [106], future studies based on larger patient cohorts are required.

Summary and future directions

The bulk of PET/MRI instrumentation research to date has focused on building MR-compatible PET detectors and readout technologies, reducing the interferences between the two imaging modalities, addressing the challenges of quantitative PET/MRI in general and MRI-guided PET attenuation correction in whole-body imaging in particular, devising tools for advanced multiparametric imaging, and finding a primary clinical role (killer application) for PET/MRI [2], [21]. In this regard, much worthwhile research in instrumentation and quantitative PET/MRI is well under way, and the technical and methodological challenges in this area are likely to be resolved in the near future. While in the clinic, radiologists and nuclear medicine physicians are in search of a primary clinical use of PET/MRI that differentiates it from PET/CT; in doing so, they are making use of tools designed for PET/CT and assessing PET/MRI in the same way as PET/CT.

In summary, the expectations for PET/MRI are high owing to the potential to obtain morphologic, functional and metabolic, qualitative, and quantitative information in the same examination. The overall consensus among active research groups is that multiparametric PET/MRI may add diagnostic certainty in difficult oncologic situations and may also help to tailor treatment plans. Recent research has shown that compared with PET/CT, PET/MRI can demonstrate equivalent lesion detection rates while offering markedly reduced radiation exposure. Although some authors [76], [79], [80], [81] have reported no added diagnostic benefit compared with PET/CT or MRI, others have described added value in selected cases. However, PET/MRI is currently still a long way from providing multiparametric information within an acceptable time window. In addition, there is no consensus regarding which parameters and how many of them are needed to influence relevant clinical endpoints, and decisional algorithms based on multiparametric data still need to be developed. Currently, the interpretation of multiparametric PET/MRI requires a team effort of imaging experts

with different backgrounds. Although this methodological approach is part of ongoing research protocols, it may be more difficult to implement in clinical everyday routine. Last but not least, cost and reimbursement issues are still a matter of debate in many countries.

To aid the implementation of PET/MRI in a clinical environment, future studies will need to address several questions: What is the advantage of PET/MRI compared with separate PET/CT and MRI, in particular, as radiation doses with recent CT scanners continue to decrease substantially? What is the value of each modality (PET, MRI, and PET/MRI) in staging and restaging, personalized treatment decisions, and treatment outcome? What are the unique key applications to PET/MRI? What is the value of multiparametric quantitative analysis tools? Only larger studies based on a solid standard of reference, such as histology and/or long-term follow-up, will be able to answer these questions.

Acknowledgments

This work was supported by the Swiss National Science Foundation under grants SNSF 31003A-_149957 and SNSF 320030_135728/1.

Authors

Habib Zaidi (habib.zaidi@hcuge.ch) is the chief physicist and head of the PET Instrumentation and Neuroimaging Laboratory at Geneva University Hospital, faculty member at the medical school of Geneva University, professor of medical physics at the University Medical Center of Groningen, and professor of molecular imaging at the University of Southern Denmark. He was guest editor for nine special issues of peer-reviewed journals and serves on the editorial board of leading journals in medical physics and molecular imaging. He is a Senior Member of the IEEE and liaison representative of the International Organization for Medical Physics to the World Health Organization. He received the 2003 Young Investigator Medical Imaging Science Award, 2004 Mark Tetalman Memorial Award, 2007 Young Scientist Prize in Biological Physics, 2010 Kuwait Prize of Applied Sciences, 2013 John S. Laughlin Young Scientist Award, 2013 Vikram Sarabhai Oration Award, and 2015 Godfrey Hounsfield Award.

Minerva Becker (minerva.becker@hcuge.ch) studied medicine at the University of Berne in Switzerland and specialized in radiology at the University Hospital in Berne. She is the past president of the European Society of Head and Neck Radiology (ESHNR), author of more than 120 scientific publications and review articles, and the recipient of more than 25 prestigious international and national scientific awards. She is a coeditor of *Valvassori's Imaging of the Head and Neck* and a reviewer for 12 scientific journals. She is currently an associate professor of radiology and the head of the Imaging Unit of Head and Neck and Maxillofacial Radiology at Geneva University Hospital. As chair of the Education Committee of the ESHNR, she is in charge of the European training curriculum in head and neck radiology and European board of head and neck radiology diploma.

References

[1] P. J. Slomka and R. P. Baum, "Multimodality image registration with software: State-of-the-art," *Eur. J. Nucl. Med. Mol. Imaging,* vol. 36, pp. 44–55, Mar. 2009.

[2] D. A. Torigian, H. Zaidi, T. C. Kwee, B. Saboury, J. K. Udupa, Z.-H. Cho, and A. Alavi, "PET/MR imaging: Technical aspects and potential clinical applications," *Radiology,* vol. 267, no. 1, pp. 26–44, Apr. 2013.

[3] H. F. Wehrl, A. W. Sauter, M. R. Divine, and B. J. Pichler, "Combined PET/MR: A technology becomes mature," *J. Nucl. Med.,* vol. 56, no. 2, pp. 165–168, Feb. 2015.

[4] H. Iida, I. Kanno, S. Miura, M. Murakami, K. Takahashi, and K. Uemura, "A simulation study of a method to reduce positron annihilation spread distribution using a strong magnetic field in positron emission tomography," *IEEE Trans. Nucl. Sci.,* vol. 33, no. 1, pp. 597–600, Feb. 1986.

[5] R. R. Raylman, B. E. Hammer, and N. L. Christensen, "Combined MRI-PET scanner: A Monte-Carlo evaluation of the improvements in PET resolution due to the effects of a static homogeneous magnetic field," *IEEE Trans. Nucl. Sci.,* vol. 43, no. 4, pp. 2406–2412, Aug. 1996.

[6] A. Wirrwar, H. Vosberg, H. Herzog, H. Halling, S. Weber, and H.-W. Muller-Gartner, "4.5 Tesla magnetic field reduces range of high-energy positrons-potential implications for positron emission tomography," *IEEE Trans. Nucl. Sci.,* vol. 44, no. 2, pp. 184–189, Apr. 1997.

[7] A. Kolb, A. W. Sauter, L. A. Eriksson, A. Vandenbrouke, C. C. Liu, C. S. Levin, B. J. Pichler, M. Rafecas, "Shine-through in PET/MRI: Effects of the magnetic field on positron range and subsequent image artifacts," *J. Nucl. Med.,* vol. 56, no. 6, pp. 951–954, June 2015.

[8] N. L. Christensen, B. E. Hammer, B. G. Heil, and K. Fetterly, "Positron emission tomography within a magnetic field using photomultiplier tubes and light-guides," *Phys. Med. Biol.,* vol. 40, no. 4, pp. 691–697, Apr. 1995.

[9] Y. Shao, S. R. Cherry, K. Farahani, and K. Meadors, "Simultaneous PET and MR imaging," *Phys. Med. Biol.,* vol. 42, no. 10, pp. 1965–1970, Oct. 1997.

[10] H. Zaidi and A. Del Guerra, "An outlook on future design of hybrid PET/MRI systems," *Med. Phys.,* vol. 38, no. 10, pp. 5667–5689, Oct. 2011.

[11] S. Yamamoto, M. Imaizumi, Y. Kanai, M. Tatsumi, M. Aoki, E. Sugiyama, M. Kawakami, E. Shimosegawa, et al., "Design and performance from an integrated PET/MRI system for small animals," *Ann. Nucl. Med.,* vol. 24, no. 2, pp. 89–98, Feb. 2010.

[12] R. C. Hawkes, T. D. Fryer, S. Siegel, R. E. Ansorge, and T. A. Carpenter, "Preliminary evaluation of a combined microPET-MR system," *Technol. Cancer Res. Treat.,* vol. 9, no. 1, pp. 53–60, Feb. 2010.

[13] W. B. Handler, K. M. Gilbert, H. Peng, and B. A. Chronik, "Simulation of scattering and attenuation of 511 keV photons in a combined PET/field-cycled MRI system," *Phys. Med. Biol.,* vol. 51, no. 10, pp. 2479–2491, May 2006.

[14] M. Bergeron, J. Cadorette, J.-F. Beaudoin, M. D. Lepage, G. Robert, V. Selivanov, M.-A. Tetrault, N. Viscogliosi, et al., "Performance evaluation of the LabPET APD-based digital PET scanner," *IEEE Trans. Nucl. Sci.,* vol. 56, no. 1, pp. 10–16, Feb. 2009.

[15] M. S. Judenhofer, H. F. Wehrl, D. F. Newport, C. Catana, S. B. Siegel, M. Becker, A. Thielscher, M. Kneilling, et al., "Simultaneous PET-MRI: A new approach for functional and morphological imaging," *Nat. Med.,* vol. 14, no. 4, pp. 459–465, Apr. 2008.

[16] B. Ravindranath, S. Junnarkar, M. Purschke, S. Stoll, X. Hong, P.-J. Huang, S. H. Maramraju, P. Vaska, et al., "Results from a simultaneous PET-MRI breast scanner [abstract]," *J. Nucl. Med.*, vol. 52, p. 432, 2011.

[17] T. W. Deller, A. M. Grant, M. M. Khalighi, S. H. Maramraju, G. Delso, and C. S. Levin, "PET NEMA performance measurements for a SiPM-based time-of-flight PET/MR system," in *2014 IEEE Nuclear Science Symp. and Medical Imaging Conf. (NSS/MIC)*, Seattle, WA.

[18] T. Frach, G. Prescher, C. Degenhardt, R. de Gruyter, A. Schmitz, and R. Ballizany, "The digital silicon photomultiplier—Principle of operation and intrinsic detector performance," in *2009 IEEE Nuclear Science Symp. Conf. Record (NSS/MIC)*, Orlando, FL, pp. 1959–1965.

[19] E. Roncali and S. R. Cherry, "Application of silicon photomultipliers to positron emission tomography," *Ann. Biomed. Eng.,* vol. 39, no. 4, pp. 1358–1377, Apr. 2011.

[20] S. Moehrs, A. Del Guerra, D. J. Herbert, and M. A. Mandelkern, "A detector head design for small-animal PET with silicon photomultipliers (SiPM)," *Phys. Med. Biol.,* vol. 51, no. 5, pp. 1113–1127, Mar. 2006.

[21] G. K. von Schulthess, F. P. Kuhn, P. Kaufmann, and P. Veit-Haibach, "Clinical positron emission tomography/magnetic resonance imaging applications," *Semin. Nucl. Med.,* vol. 43, no. 1, pp. 3–10, Jan. 2013.

[22] P. Vaska and T. Cao, "The state of instrumentation for combined positron emission tomography and magnetic resonance imaging," *Semin. Nucl. Med.,* vol. 43, no. 1, pp. 11–18, Jan. 2013.

[23] H. Zaidi, "A pivotal time for hybrid PET/MR imaging technology," *J. Am. Coll. Radiol.,* vol. 10, no. 11, pp. 878–881, Nov. 2013.

[24] H. Zaidi, N. Ojha, M. Morich, J. Griesmer, Z. Hu, P. Maniawski, O. Ratib, D. Izquierdo-Garcia, et al., "Design and performance evaluation of a whole-body

Ingenuity TF PET-MRI system," *Phys. Med. Biol.,* vol. 56, no. 10, pp. 3091–3106, May 2011.

[25] P. Veit-Haibach, F. P. Kuhn, F. Wiesinger, G. Delso, and G. von Schulthess, "PET–MR imaging using a tri-modality PET/CT–MR system with a dedicated shuttle in clinical routine," *MAGMA*, vol. 26, no. 1, pp. 25–35, Feb. 2013.

[26] Z. H. Cho, Y. D. Son, H. K. Kim, K. N. Kim, S. H. Oh, J. Y. Han, I. K. Hong, and Y. B. Kim, "A fusion PET-MRI system with a high-resolution research tomograph-PET and ultra-high field 7.0 T-MRI for the molecular-genetic imaging of the brain," *Proteomics,* vol. 8, no. 6, pp. 1302–1323, Mar. 2008.

[27] H. P. Schlemmer, B. J. Pichler, M. Schmand, Z. Burbar, C. Michel, R. Ladebeck, K. Jattke, D. Townsend, et al., "Simultaneous MR/PET imaging of the human brain: Feasibility study," *Radiology,* vol. 248, no. 3, pp. 1028–1035, Sept. 2008.

[28] A. Boss, A. Kolb, M. Hofmann, S. Bisdas, T. Nagele, U. Ernemann, L. Stegger, C. Rossi, et al., "Diffusion tensor imaging in a human PET/MR hybrid system," *Invest. Radiol.,* vol. 45, no. 5, pp. 270–274, May 2010.

[29] G. Delso, S. Fürst, B. Jakoby, R. Ladebeck, C. Ganter, S. G. Nekolla, M. Schwaiger, and S. I. Ziegler, "Performance measurements of the Siemens mMR integrated whole-body PET/MR scanner," *J. Nucl. Med.,* vol. 52, no. 12, pp. 1914–1922, Dec. 2011.

[30] A. Kolb, H. F. Wehrl, M. Hofmann, M. S. Judenhofer, L. Eriksson, R. Ladebeck, M. P. Lichy, L. Byars, et al., "Technical performance evaluation of a human brain PET/MRI system," *Eur. Radiol.,* vol. 22, no. 8, pp. 1776–1788, Aug. 2012.

[31] A. Martinez-Möller, M. Eiber, S. G. Nekolla, M. Souvatzoglou, A. Drzezga, S. Ziegler, E. J. Rummeny, M. Schwaiger, et al., "Workflow and scan protocol considerations for integrated whole-body PET/MRI in oncology," *J. Nucl. Med.,* vol. 53, no. 9, pp. 1415–1426, Sept. 2012.

[32] A. Mehranian and H. Zaidi, "Impact of time-of-flight PET on quantification errors in MRI-based attenuation correction," *J. Nucl. Med.,* vol. 56, no. 4, pp. 635–641, Apr. 2015.

[33] D. R. Schaart, S. Seifert, R. Vinke, H. T. van Dam, P. Dendooven, H. Löhner, and F. J. Beekman, "LaBr(3):Ce and SiPMs for time-of-flight PET: Achieving 100 ps coincidence resolving time," *Phys. Med. Biol.,* vol. 55, no. 7, pp. N179–N189, Apr. 2010.

[34] M. V. Nemallapudi, S. Gundacker, P. Lecoq, E. Auffray, A. Ferri, A. Gola, and C. Piemonte, "Sub-100 ps coincidence time resolution for positron emission tomography with LSO:Ce codoped with Ca," *Phys. Med. Biol.,* vol. 60, no. 12, pp. 4635–4649, June 2015.

[35] M. S. Judenhofer and S. R. Cherry, "Applications for preclinical PET/MRI," *Semin. Nucl. Med.,* vol. 43, no. 1, pp. 19–29, Jan. 2013.

[36] H. Zaidi, "Is MRI-guided attenuation correction a viable option for dual-modality PET/MR imaging?," *Radiology,* vol. 244, no. 3, pp. 639–642, Sept. 2007.

[37] A. Mehranian, H. Arabi, and H. Zaidi, "Magnetic resonance imaging-guided attenuation correction in PET/MRI: Challenges, solutions and opportunities," *Med. Phys.*, vol. 43, no. 3, pp. 1130–1155, Mar. 2016.

[38] Y. Berker, J. Franke, A. Salomon, M. Palmowski, H. C. Donker, Y. Temur, F. M. Mottaghy, C. Kuhl, et al., "MRI-based attenuation correction for hybrid PET/MRI systems: A 4-class tissue segmentation technique using a combined ultrashort-echo-time/Dixon MRI sequence," *J. Nucl. Med.,* vol. 53, no. 5, pp. 796–804, May 2012.

[39] G. Delso, F. Wiesinger, L. Sacolick, S. Kaushik, D. Shanbhag, M. Hüllner, and P. Veit-Haibach, "Clinical evaluation of zero echo time MRI for the segmentation of the skull," *J. Nucl. Med.,* vol. 56, no. 3, pp. 417–422, Mar. 2015.

[40] A. Martinez-Möller, M. Souvatzoglou, G. Delso, R. A. Bundschuh, C. Chefd'hotel, S. I. Ziegler, N. Navab, M. Schwaiger, et al., "Tissue classification as a potential approach for attenuation correction in whole-body PET/MRI: Evaluation with PET/CT data," *J. Nucl. Med.,* vol. 50, no. 4, pp. 520–526, Apr. 2009.

[41] J. Ouyang, S. Y. Chun, Y. Petibon, A. A. Bonab, N. Alpert, and G. El Fakhri, "Bias atlases for segmentation-based PET attenuation correction using PET-CT and MR," *IEEE Trans. Nucl. Sci.,* vol. 60, no. 5, pp. 3373–3382, Oct. 2013.

[42] A. Akbarzadeh, M. R. Ay, A. Ahmadian, N. Riahi Alam, and H. Zaidi, "MRI-guided attenuation correction in whole-body PET/MR: Assessment of the effect of bone attenuation," *Ann. Nucl. Med.,* vol. 27, no. 2, pp. 152–162, Feb. 2013.

[43] M. C. Aznar, R. Sersar, J. Saabye, C. N. Ladefoged, F. L. Andersen, J. H. Rasmussen, J. Löfgren, and T. Beyer, "Whole-body PET/MRI: The effect of bone attenuation during MR-based attenuation correction in oncology imaging," *Eur. J. Radiol.,* vol. 83, no. 7, pp. 1177–1183, July 2014.

[44] H. Arabi, O. Rager, A. Alem, A. Varoquaux, M. Becker, and H. Zaidi, "Clinical assessment of MR-guided 3-class and 4-class attenuation correction in PET/MR," *Mol. Imaging Biol.,* vol. 17, no. 2, pp. 264–276, Apr. 2015.

[45] D. H. Paulus, H. H. Quick, C. Geppert, M. Fenchel, Y. Zhan, G. Hermosillo, D. Faul, F. Boada, et al., "Whole-body PET/MR imaging: Quantitative evaluation of a novel model-based MR attenuation correction method including bone," *J. Nucl. Med.*, vol. 56, no. 7, pp. 1061–1066, July 2015.

[46] M. Hofmann, I. Bezrukov, F. Mantlik, P. Aschoff, F. Steinke, T. Beyer, B. J. Pichler, and B. Scholköpf, "MRI-based attenuation correction for whole-body PET/MRI: Quantitative evaluation of segmentation- and atlas-based methods," *J. Nucl. Med.,* vol. 52, no. 9, pp. 1392–1399, Sept. 2011.

[47] E. Schreibmann, J. A. Nye, D. M. Schuster, D. R. Martin, J. Votaw, and T. Fox, "MR-based attenuation correction for hybrid PET-MR brain imaging systems using deformable image registration," *Med. Phys.,* vol. 37, no. 5, pp. 2101–2109, May 2010.

[48] N. Burgos, M. J. Cardoso, K. Thielemans, M. Modat, S. Pedemonte, J. Dickson, A. Barnes, R. Ahmed, et al., "Attenuation correction synthesis for hybrid PET-MR scanners: Application to brain studies," *IEEE Trans. Med. Imaging*, vol. 33, no. 12, pp. 2332–2341, Dec. 2014.

[49] M. R. Juttukonda, B. G. Mersereau, Y. Chen, Y. Su, B. G. Rubin, T. L. Benzinger, D. S. Lalush, and H. An, "MR-based attenuation correction for PET/MRI neurological studies with continuous-valued attenuation coefficients for bone through a conversion from R2* to CT-Hounsfield units," *NeuroImage,* vol. 112, pp. 160–168, May 2015.

[50] H. Arabi and H. Zaidi, "Fast atlas-based MRI-guided PET attenuation map generation in whole-body PET/MR imaging," in *2015 IEEE Nuclear Science Symp. and Medical Imaging Conf. (NSS/MIC)*, San Diego, CA, 2015.

[51] A. Rezaei, M. Defrise, G. Bal, C. Michel, M. Conti, C. Watson, and J. Nuyts, "Simultaneous reconstruction of activity and attenuation in time-of-flight PET," *IEEE Trans. Med. Imaging,* vol. 31, no. 12, pp. 2224–2233, Dec. 2012.

[52] A. Salomon, A. Goedicke, B. Schweizer, T. Aach, and V. Schulz, "Simultaneous reconstruction of activity and attenuation for PET/MR," *IEEE Trans. Med. Imaging,* vol. 30, no. 3, pp. 804–813, Mar. 2011.

[53] A. Mehranian and H. Zaidi, "Joint estimation of activity and attenuation in whole-body TOF PET/MRI using constrained Gaussian mixture models," *IEEE Trans. Med. Imaging,* vol. 34, no. 9, pp. 1808–1821, Sept. 2015.

[54] A. Mehranian and H. Zaidi, "Clinical assessment of emission- and segmentation-based MRI-guided attenuation correction in whole body TOF PET/MRI," *J. Nucl. Med.,* vol. 56, no. 6, pp. 877–883, June 2015.

[55] A. J. Reader and H. Zaidi, "Advances in PET image reconstruction," *PET Clinics,* vol. 2, no. 2, pp. 173–190, Apr. 2007.

[56] P. J. Green, "Bayesian reconstructions from emission tomography data using a modified EM algorithm," *IEEE Trans. Med. Imaging,* vol. 9, no. 1, pp. 84–93, Mar. 1990.

[57] B. Bai, Q. Li, and R. M. Leahy, "Magnetic resonance-guided positron emission tomography image reconstruction," *Semin. Nucl. Med.,* vol. 43, no. 1, pp. 30–44, Jan. 2013.

[58] K. Baete, J. Nuyts, W. Van Paesschen, P. Suetens, and P. Dupont, "Anatomical-based FDG-PET reconstruction for the detection of hypo-metabolic regions in epilepsy," *IEEE Trans. Med. Imaging,* vol. 23, no. 4, pp. 510–519, Apr. 2004.

[59] J. Tang and A. Rahmim, "Bayesian PET image reconstruction incorporating anato-functional joint entropy," *Phys. Med. Biol.,* vol. 54, no. 23, pp. 7063–7075, Dec. 2009.

[60] K. Erlandsson, I. Buvat, P. H. Pretorius, B. A. Thomas, and B. F. Hutton, "A review of partial volume correction techniques for emission tomography and their applications in neurology, cardiology and oncology," *Phys. Med. Biol.,* vol. 57, no. 21, pp. R119–R159, Nov. 2012.

[61] M. Quarantelli, K. Berkouk, A. Prinster, B. Landeau, C. Svarer, L. Balkay, B. Alfano, A. Brunetti, et al., "Integrated software for the analysis of brain PET/SPECT studies with partial-volume-effect correction," *J. Nucl. Med.,* vol. 45, no. 2, pp. 192–201, Feb. 2004.

[62] H. Matsuda, T. Ohnishi, T. Asada, Z. J. Li, H. Kanetaka, E. Imabayashi, F. Tanaka, and S. Nakano, "Correction for partial-volume effects on brain perfusion SPECT in healthy men," *J. Nucl. Med.,* vol. 44, no. 8, pp. 1243–1252, Aug. 2003.

[63] H. Zaidi, T. Ruest, F. Schoenahl, and M.-L. Montandon, "Comparative evaluation of statistical brain MR image segmentation algorithms and their impact on partial volume effect correction in PET," *NeuroImage,* vol. 32, no. 4, pp. 1591–1607, Oct. 2006.

[64] V. Frouin, C. Comtat, A. Reilhac, and M.-C. Grégoire, "Correction of partial volume effect for PET striatal imaging: Fast implementation and study of robustness," *J. Nucl. Med.,* vol. 43, no. 12, pp. 1715–1726, Dec. 2002.

[65] M. Shidahara, C. Tsoumpas, A. Hammers, N. Boussion, D. Visvikis, T. Suhara, I. Kanno, and F. E. Turkheimer, "Functional and structural synergy for resolution recovery and partial volume correction in brain PET," *NeuroImage,* vol. 44, no. 2, pp. 340–348, Jan. 2009.

[66] C. Catana, "Motion correction options in PET/MRI," *Semin. Nucl. Med.,* vol. 45, no. 3, pp. 212–223, May 2015.

[67] A. J. van der Kouwe, T. Benner, and A. M. Dale, "Real-time rigid body motion correction and shimming using cloverleaf navigators," *Magn. Reson. Med.,* vol. 56, no. 5, pp. 1019–1032, Nov. 2006.

[68] C. Catana, T. Benner, A. van der Kouwe, L. Byars, M. Hamm, D. B. Chonde, C. J. Michel, G. El Fakhri, et al., "MRI-assisted PET motion correction for neurologic studies in an integrated MR-PET scanner," *J. Nucl. Med.,* vol. 52, no. 1, pp. 154–161, Jan. 2011.

[69] C. Tsoumpas, J. E. Mackewn, P. Halsted, A. P. King, C. Buerger, J. J. Totman, T. Schaeffter, and P. K. Marsden, "Simultaneous PET-MR acquisition and

MR-derived motion fields for correction of non-rigid motion in PET," *Ann. Nucl. Med.,* vol. 24, no. 10, pp. 745–750, Dec. 2010.

[70] P. Kellman, C. Chefd'hotel, C. H. Lorenz, C. Mancini, A. E. Arai, and E. R. McVeigh, "Fully automatic, retrospective enhancement of real-time acquired cardiac cine MR images using image-based navigators and respiratory motion-corrected averaging," *Magn. Reson. Med.,* vol. 59, no. 4, pp. 771–778, Apr. 2008.

[71] A. H. Davarpanah, Y. P. Chen, A. Kino, C. T. Farrelly, A. N. Keeling, J. J. Sheehan, A. B. Ragin, P. J. Weale, et al., "Accelerated two- and three-dimensional cine MR imaging of the heart by using a 32-channel coil," *Radiology,* vol. 254, no. 1, pp. 98–108, Jan. 2010.

[72] B. Guerin, S. Cho, S. Y. Chun, X. Zhu, N. M. Alpert, G. El Fakhri, T. Reese, and C. Catana, "Nonrigid PET motion compensation in the lower abdomen using simultaneous tagged-MRI and PET imaging," *Med. Phys.*, vol. 38, no. 6, pp. 3025–3038, June 2011.

[73] S. Y. Chun, T. G. Reese, J. Ouyang, B. Guerin, C. Catana, X. Zhu, N. M. Alpert, and G. El Fakhri, "MRI-based nonrigid motion correction in simultaneous PET/MRI," *J. Nucl. Med.,* vol. 53, no. 8, pp. 1284–1291, Aug. 2012.

[74] A. P. King, C. Buerger, C. Tsoumpas, P. K. Marsden, and T. Schaeffter, "Thoracic respiratory motion estimation from MRI using a statistical model and a 2-D image navigator," *Med. Image Anal.,* vol. 16, no. 1, pp. 252–264, Jan. 2012.

[75] H. Fayad, H. Schmidt, C. Wuerslin, and D. Visvikis, "Reconstruction-incorporated respiratory motion correction in clinical simultaneous PET/MR imaging for oncology applications," *J. Nucl. Med.,* vol. 56, no. 6, pp. 884–889, June 2015.

[76] A. Varoquaux, O. Rager, A. Poncet, B. M. Delattre, O. Ratib, C. D. Becker, P. Dulguerov, N. Dulguerov, et al., "Detection and quantification of focal uptake in head and neck tumours: 18F-FDG PET/MR versus PET/CT," *Eur. J. Nucl. Med. Mol. Imaging,* vol. 41, no. 3, pp. 462–475, Mar. 2014.

[77] M. I. Vargas, M. Becker, V. Garibotto, S. Heinzer, P. Loubeyre, J. Gariani, K. Lovblad, J. P. Vallée, et al., "Approaches for the optimization of MR protocols in clinical hybrid PET/MRI studies," *MAGMA,* vol. 26, no. 1, pp. 57–69, Feb. 2013.

[78] A. Drzezga, M. Souvatzoglou, M. Eiber, A. Beer, S. Ziegler, S. Furst, A. Martinez-Möller, S. G. Nekolla, et al., "First clinical experience with integrated whole-body MR/PET. Comparison to PET/CT in patients with oncological diagnoses," *J. Nucl. Med.,* vol. 53, no. 6, pp. 845–855, June 2012.

[79] K. Kubiessa, S. Purz, M. Gawlitza, A. Kuhn, J. Fuchs, K. G. Steinhoff, A. Boehm, O. Sabri, et al., "Initial clinical results of simultaneous 18F-FDG PET/MRI in comparison to 18F-FDG PET/CT in patients with head and neck cancer," *Eur. J. Nucl. Med. Mol. Imaging,* vol. 41, no. 4, pp. 639–648, Apr. 2014.

[80] I. Platzek, B. Beuthien-Baumann, M. Schneider, V. Gudziol, H. H. Kitzler, J. Maus, G. Schramm, M. Popp, et al., "FDG PET/MR for lymph node staging in head and neck cancer," *Eur. J. Radiol.,* vol. 83, no. 7, pp. 1163–1168, July 2014.

[81] S. Taneja, A. Jena, R. Goel, R. Sarin, and S. Kaul, "Simultaneous whole-body 18F-FDG PET-MRI in primary staging of breast cancer: A pilot study," *Eur. J. Radiol.,* vol. 83, no. 12, pp. 2231–2239, Dec. 2014.

[82] T. de Perrot, O. Rager, M. Scheffler, M. Lord, M. Pusztaszeri, C. Iselin, O. Ratib, and J. P. Vallée, et al., "Potential of hybrid F-fluorocholine PET/MRI for prostate cancer imaging," *Eur. J. Nucl. Med. Mol. Imaging,* vol. 41, no. 9, pp. 1744–1755, Sept. 2014.

[83] B. S. Purohit, P. Dulguerov, K. Burkhardt, and M. Becker, "Dedifferentiated laryngeal chondrosarcoma: Combined morphologic and functional imaging with positron-emission tomography/magnetic resonance imaging," *Laryngoscope*, vol. 124, no. 7, pp. E274–E277, July 2014.

[84] K. J. Beiderwellen, T. D. Poeppel, V. Hartung-Knemeyer, C. Buchbender, H. Kuehl, A. Bockisch, and T. C. Lauenstein, "Simultaneous ^{68}Ga-DOTATOC PET/MRI in patients with gastroenteropancreatic neuroendocrine tumors: Initial results," *Invest. Radiol.,* vol. 48, no. 5, pp. 273–279, May 2013.

[85] B. S. Purohit, A. Ailianou, N. Dulguerov, C. D. Becker, O. Ratib, and M. Becker, "FDG-PET/CT pitfalls in oncological head and neck imaging," *Insights Imaging,* vol. 5, no. 5, pp. 585–602, Oct. 2014.

[86] M. Becker and H. Zaidi, "Imaging in head and neck squamous cell carcinoma: The potential role of PET/MRI," *Br. J. Radiol.,* vol. 87, no. 1036, 20130677, Apr. 2014.

[87] D. L. Bailey, G. Antoch, P. Bartenstein, H. Barthel, A. J. Beer, S. Bisdas, D. A. Bluemke, R. Boellaard, et al., "Combined PET/MR: The real work has just started. Summary report of the third international workshop on PET/MR imaging; February 17–21, 2014, Tübingen, Germany," *Mol. Imaging Biol.* vol 17, no. 3, pp. 297–312, June 2015.

[88] S. Purz, O. Sabri, A. Viehweger, H. Barthel, R. Kluge, I. Sorge, and F. W. Hirsch, "Potential pediatric applications of PET/MR," *J. Nucl. Med.,* vol. 55, pp. 32S–39S, Apr. 2014.

[89] J. Gu, T. Chan, J. Zhang, A. Y. Leung, Y. L. Kwong, and P. L. Khong, "Whole-body diffusion-weighted imaging: The added value to whole-body MRI at initial diagnosis of lymphoma," *AJR Am. J. Roentgenol.,* vol. 197, no. 3, pp. W384–W391, Sept. 2011.

[90] C. Lin, A. Luciani, E. Itti, C. Haioun, V. Safar, M. Meignan, and A. Rahmouni, "Whole-body diffusion magnetic resonance imaging in the assessment of lymphoma," *Cancer Imaging,* vol. 12, no. 2, pp. 403–408, Sept. 2012.

[91] S. Punwani, S. A. Taylor, Z. Z. Saad, A. Bainbridge, A. Groves, S. Daw, A. Shankar, S. Halligan, et al., "Diffusion-weighted MRI of lymphoma: Prognostic utility and implications for PET/MRI?," *Eur. J. Nucl. Med. Mol. Imaging,* vol. 40, no. 3, pp. 373–385, Feb. 2013.

[92] A. Varoquaux, O. Rager, K. O. Lovblad, K. Masterson, P. Dulguerov, O. Ratib, C. D. Becker, and M. Becker, "Functional imaging of head and neck squamous cell carcinoma with diffusion-weighted MRI and FDG PET/CT: Quantitative analysis of ADC and SUV," *Eur. J. Nucl. Med. Mol. Imaging,* vol. 40, no. 6, pp. 842–852, June 2013.

[93] F. P. Kuhn, M. Hüllner, C. E. Mader, N. Kastrinidis, G. F. Huber, G. K. von Schulthess, S. Kollias, and P. Veit-Haibach, "Contrast-enhanced PET/MR imaging versus contrast-enhanced PET/CT in head and neck cancer: How much MR information is needed?," *J. Nucl. Med.,* vol. 55, no. 4, pp. 551–558, Apr. 2014.

[94] M. Comoretto, L. Balestreri, E. Borsatti, M. Cimitan, G. Franchin, and M. Lise, "Detection and restaging of residual and/or recurrent nasopharyngeal carcinoma after chemotherapy and radiation therapy: Comparison of MR imaging and FDG PET/CT," *Radiology,* vol. 249, no. 1, pp. 203–211, Oct. 2008.

[95] S. Punwani, K. K. Cheung, N. Skipper, N. Bell, A. Bainbridge, S. A. Taylor, A. M. Groves, S. F. Hain, et al., "Dynamic contrast-enhanced MRI improves accuracy for detecting focal splenic involvement in children and adolescents with Hodgkin disease," *Pediatr. Radiol.,* vol. 43, no. 8, pp. 941–949, Aug. 2013.

[96] J. F. Schäfer, S. Gatidis, H. Schmidt, B. Guckel, I. Bezrukov, C. A. Pfannenberg, M. Reimold, M. Ebinger, et al., "Simultaneous whole-body PET/MR imaging in comparison to PET/CT in pediatric oncology: Initial results," *Radiology,* vol. 273, no. 1, pp. 220–231, Oct. 2014.

[97] C. Martinez-Rios, R. F. Muzic, Jr., F. P. DiFilippo, L. Hu, C. Rubbert, and K. A. Herrmann, "Artifacts and diagnostic pitfalls in positron emission tomography-magnetic resonance imaging," *Semin. Roentgenol.,* vol. 49, no. 3, pp. 255–270, June 2014.

[98] G. Delso, A. Martinez-Möller, R. A. Bundschuh, S. G. Nekolla, and S. I. Ziegler, "The effect of limited MR field of view in MR/PET attenuation correction," *Med. Phys.,* vol. 37, no. 6, pp. 2804–2812, June 2010.

[99] U. Attenberger, C. Catana, H. Chandarana, O. A. Catalano, K. Friedman, S. A. Schonberg, J. Thrall, M. Salvatore, et al., "Whole-body FDG PET-MR oncologic imaging: Pitfalls in clinical interpretation related to inaccurate MR-based attenuation correction," *Abdom. Imaging,* vol. 40, no. 6, pp. 1374–1386, Aug. 2015.

[100] C. B. Brendle, H. Schmidt, S. Fleischer, U. H. Braeuning, C. A. Pfannenberg, and N. F. Schwenzer, "Simultaneously acquired MR/PET images compared with sequential MR/PET and PET/CT: Alignment quality," *Radiology,* vol. 268, no. 1, pp. 190–199, July 2013.

[101] N. F. Osman and J. L. Prince, "Regenerating MR tagged images using harmonic phase (HARP) methods," *IEEE Trans. Biomed. Eng.,* vol. 51, no. 8, pp. 1428–1433, Aug. 2004.

[102] R. Manber, K. Thielemans, B. F. Hutton, A. Barnes, S. Ourselin, S. Arridge, C. O'Meara, S. Wan, et al., "Practical PET respiratory motion correction in clinical PET/MR," *J. Nucl. Med.,* vol. 56, no. 6, pp. 890–896, June 2015.

[103] R. Sutter, E. J. Ulbrich, V. Jellus, M. Nittka, and C. W. Pfirrmann, "Reduction of metal artifacts in patients with total hip arthroplasty with slice-encoding metal artifact correction and view-angle tilting MR imaging," *Radiology,* vol. 265, no. 1, pp. 204–214, Oct. 2012.

[104] C. N. Ladefoged, F. L. Andersen, S. H. Keller, T. Beyer, I. Law, L. Højgaard, S. Darkner, and F. Lauze, "Automatic correction of dental artifacts in PET/MRI," *J. Med. Imaging (Bellingham),* vol. 2, no. 2, 024009, Apr. 2015.

[105] C. Lois, I. Bezrukov, H. Schmidt, N. Schwenzer, M. Werner, J. Kupferschläger, and T. Beyer, "Effect of MR contrast agents on quantitative accuracy of PET in combined whole-body PET/MR imaging," *Eur. J. Nuc. Med. Mol. Imaging,* vol. 39, no. 11, pp. 1756–1766, Nov. 2012.

[106] A. Varoquaux, O. Rager, P. Dulguerov, K. Burkhardt, A. Ailianou, and M. Becker, "Diffusion-weighted and PET/MR imaging after radiation therapy for malignant head and neck tumors," *RadioGraphics*, vol. 35, no. 5, pp. 1502–1527, Sept.–Oct. 2015.

[107] P. Heusch, C. Sproll, C. Buchbender, E. Rieser, J. Terjung, C. Antke, I. Boeck, S. Macht, et al., "Diagnostic accuracy of ultrasound, ^{18}F-FDG-PET/CT, and fused ^{18}F-FDG-PET-MR images with DWI for the detection of cervical lymph node metastases of HNSCC," *Clin. Oral Investig.,* vol. 18, no. 3, pp. 969–978, Apr. 2014.

[108] H. Chandarana, L. Heacock, R. Rakheja, L. R. Demello, J. Bonavita, T. K. Block, C. Geppert, J. S. Babb, et al., "Pulmonary nodules in patients with primary malignancy: Comparison of hybrid PET/MR and PET/CT imaging," *Radiology,* vol. 268, no. 3, pp. 874–881, Sept. 2013.

SP